

Review

Current understanding and challenges in high temperature additive manufacturing of engineering thermoplastic polymers



Arit Das^{a,b,1}, Camden A. Chatham^{a,c,1}, Jacob J. Fallon^{a,c}, Callie E. Zawaski^{a,d}, Eric L. Gilmer^{a,b}, Christopher B. Williams^{a,d,*}, Michael J. Bortner^{a,b,**}

^a Macromolecules Innovation Institute, Virginia Tech, Blacksburg, VA, 24061, USA

^b Department of Chemical Engineering, Virginia Tech, Blacksburg, VA 24061, USA

^c Macromolecular Science and Engineering, Virginia Tech, Blacksburg, VA 24061, USA

^d Department of Mechanical Engineering, Virginia Tech, Blacksburg, VA 24061, USA

ARTICLE INFO

Keywords:

3D printing
Material extrusion
Powder bed fusion
Thermoplastic processing
High temperature engineering thermoplastics

ABSTRACT

The strengths of additive manufacturing (AM), especially the tool-less manufacturing paradigm and rapid production of low-volume products, are well-aligned with the needs of manufacturing of expensive, high-temperature resistant, engineering thermoplastic polymers. High temperature polymer parts made with AM for either tooling or end-use applications have been implemented in the aerospace, automotive, and biomedical fields. However, parts made from these polymers using traditional manufacturing processes are generally high-value parts in low-quantity production runs. Moreover, AM processing of these polymers present significant challenges due to limitations associated with large thermal gradients, residual stress buildup, and interlayer adhesion as well as the inability of the printers to consistently maintain required high processing temperatures. This review highlights the current state of the art for processing high-temperature (i.e., traditional processing temperatures exceeding 250°C) thermoplastic polymers by the melt-based, AM processes of material extrusion (MatEx) and laser powder bed fusion (PBF). The authors address common challenges to AM of high-temperature polymers and gaps in fundamental understanding of the process-structure-property relationships needed to identify the machine design, process parameter selection, and synthetic modifications to enable processing.

1. Introduction

Currently, polymer-based AM is predominantly used in prototype development and functional testing of fixtures and tools to provide a certain degree of performance assurance before investing in injection-molding tooling [1–3]. Moreover, it is also used for the manufacture of

small-scale parts for non-load bearing applications such as brackets, wire harnesses, ducts, etc. [4]. However, with the rapid development of high-performance polymeric materials, polymer based AM has been used in the manufacture of medical implants, optical products, architectural parts, sports equipment, smart textiles, and soft robotics [5–8]. There are also applications like custom tools for aerospace industries

Abbreviations: E_A , activation energy for degradation; AM, additive manufacturing; A, area of a filament; a_0 , average particle size; v_s , beam speed; T_b , bed temperature; BAAM, big area additive manufacturing; CB, carbon black; CF, carbon fiber; CNF, carbon nanofiber; CNT, carbon nanotube; λ , characteristic relaxation time; CTE, coefficient of thermal expansion; CAE, computer aided engineering; d_L , diameter of laser beam; DOE, design of experiments; DSC, differential scanning calorimetry; E_d , energy density; EMR, energy melt ratio; EMR_{deg} , energy melt ratio before degradation; v_f , feed velocity; F, force to drive a filament across nozzle; GF, glass fiber; T_g , glass transition temperature; GNP, graphene nanoplatelet; h_s , hatch spacing; HSS, high speed sintering; P_L , laser power; LAMPS, laser additive manufacturing pilot system; h_f , latent heat of fusion; Q, material density; MatEx, material extrusion; T_m , melting temperature; P_M , motor power; MJF, Multi-jet fusion; L, nozzle length; Φ , packing ratio of powder bed; PA, polyamide; PAEK, polyaryl ether ketone; PC, polycarbonate; PEK, poly ether ketone; PEEK, poly ether ether ketone; PEI, poly ether imide; PEKK, poly ether ketone ketone; PPS, poly phenylene sulfide; PPSU, poly phenyl sulfone; PBF, powder bed fusion; ΔP , pressure drop across nozzle; R_f , radius of filament; R_N , radius of nozzle; RSM, response surface methodology; C_p , specific heat capacity; Γ , surface tension; TLCP, thermotropic liquid crystalline polymer; $T_{d,1\%}$, temperature at 1% weight loss; η , viscosity of polymer melt; V , volumetric flow rate; M_w , weight average molecular weight; η_0 , zero shear melt viscosity

* Corresponding author at: Macromolecules Innovation Institute and Department of Mechanical Engineering, Virginia Tech, Blacksburg, VA, 24061, USA.

** Corresponding author at: Macromolecules Innovation Institute and Department of Chemical Engineering, Virginia Tech, Blacksburg, VA, 24061, USA.

E-mail addresses: cbwill@vt.edu (C.B. Williams), mj.bortner@vt.edu (M.J. Bortner).

¹ These authors contributed equally to the work

which are using parts manufactured by AM [9]. But there are still concerns regarding the consistency and repeatability in the part properties manufactured by AM since the evolution of properties during AM processing is yet to be completely understood [10]. In order to expand the polymer material catalog for AM, it is suggested to move away from materials tailored for traditional processing techniques and come up with *a-priori* design of polymers that accounts for the complex multi-physics and kinetics associated with the AM process. This “molecules (polymer design and synthesis) to manufacturing (using AM)” approach can lead to rapid progress toward fully understanding the complex field of AM based technologies.

At present, a high percentage of consumer and commercial commodities are manufactured using thermoplastic materials. Already, the aerospace, biomedical, and automotive industries have become early adopters of this technology beyond prototyping for the production of intermediate tooling and end-use parts. These early-adopter industries often use thermoplastic polymers for mechanical impact and bio-inert properties in addition to their ease of processing using traditional means. In addition, these industries often require their products to work at elevated temperatures, in the presence of flames and harsh solvents, and under high mechanical loads. Therefore, high temperature engineering polymers are well-suited for these early adopter industries. In the scope of this paper, we focus on “high-temperature engineering thermoplastic materials”, meaning those polymers with processing temperature requirements higher than 250°C.

Processing high-temperature engineering thermoplastics has additional challenges specific to processing at high temperatures. High-temperature processing challenges can be categorized as either machine- or material-based. Material-based challenges arise from the chemical complexities in synthesizing polymers of highly thermally-stable bonds capable of surviving both the needs for the target application and the necessarily more extreme conditions of the manufacturing environment. As polymer processing occurs significantly above the polymer’s glass transition temperature (T_g), lengthy processing times have the potential to alter the molecular structure or architecture of any given polymer, thereby changing the properties of the fabricated part. It is, therefore, important to understand how processing affects the molecular structure to generate accurate predictions of final part properties. Machine-based challenges for high-temperature processing often center on the selective delivery of energy to the target material being processed and preferentially away from sensitive components of the manufacturing equipment, especially electronic components. Addressing these challenges requires significant additional investment in machine design and utilization of either insulating materials or electronic components rated for sustained use at elevated temperatures.

As thermoplastic polymers have historically been processed through melt-and-form/reform manufacturing techniques (e.g., injection molding, thermoforming, rotational molding, etc.), it is natural for those AM technologies using similar melt-and-form techniques to form layers, i.e., melt-based material extrusion (MatEx) and powder bed fusion (PBF), to be utilized when printing this valuable class of polymers. There are a few instances of high-performance polymers being printed via other AM techniques, such as vat photopolymerization [11]; however, these techniques do not extensively appear in published research or in commercial application. Melt-based manufacturing techniques are primarily directed by thermal and rheological polymer properties. Therefore, experimental techniques evaluating polymer melt and crystallization behavior, temperature- and shear-dependent flow behavior, coefficient of thermal expansion (CTE), and thermal conductivity are critical to understanding how these polymers respond to the varied stimuli at each stage of the AM process.

The growth opportunity for this form of advanced manufacturing is predicated on the state-of-the-art understanding of process physics governing 3D printing of high-temperature engineering thermoplastic polymers. The aim of this paper is to provide a summary of the state-of-

the-art of high-temperature thermoplastic polymer printing, highlighting key differences in processing with AM that present unique challenges, and discussing observed research trends and gaps in the governing process physics of AM specific to high-temperature polymers.

2. Roadmap

Many review papers have been authored in recent years synthesizing published knowledge toward a specific aspect of AM. Several such reviews focus on reporting the materials available for each of the different AM technology families [12–15]. Reviews, including the ones authored by Bourell, et al. [12] and Ligon, et al. [13], provide overviews for how existing materials are formulated, printed, and used. These reviews, however, have a broad focus and do not focus on any particular AM subset or classification of polymers. Other reviews narrow their focus either to one AM process [16–18], but include all polymer families, or a particular application for additively manufactured parts [19–22].

This review has the narrowed focus of discussing the unique challenges of a subset class of polymeric materials resulting from the structure-property-processing relationships present in PBF and MatEx AM. Other published reviews have focused on manufacturing relationships in other subsets of polymeric materials, such as Peterson’s review on ABS in MatEx [23], Wang and coauthors’ review of polymer composites [24], and Yuan and coauthors’ review of polymeric powder composites [25]; however, the authors are unaware of any other reviews focusing on high-temperature thermoplastics for AM. As an impetus for this literature survey, recent review articles offer quite limited discussions of available high temperature engineering thermoplastic polymers for PBF and MatEx.

The authors have arranged this paper to provide an initial, high-level overview of high-temperature polymers in AM, followed by sections specific to each high-temperature polymer that has been printed to date. These polymer-specific discussion sections summarize the reported successful printing of each polymer and offer discussion on example use-cases that utilize both an advantage given by the polymer’s properties and an advantage uniquely provided by printing that polymer either by PBF or MatEx. The processing physics are also discussed to highlight current opportunities for additional research. The authors conclude this manuscript by discussing the importance of continued investigation into the structure-property-process relationships in polymer AM.

3. Overview of process-structure-property relationships between AM and high temperature engineering polymers

3.1. Powder bed fusion: Process

PBF based AM was developed at the University of Texas at Austin in the 1980s [26]. Despite revisions and modifications over the years, the technology has always been comprised of three sub-functions: (1) powder recoating, (2) energy input, and (3) coalescence and cooling. The authors have previously published a review article describing in great detail what is known regarding the structure-property-processing relationships in PBF, including distinctions among the PBF sub-technologies of laser sintering, high-speed sintering (HSS), and multi-jet fusion (MJF) [17]. This paper focuses exclusively on laser sintering as processing high-temperature polymers via HSS or MJF are not extensively reported. Table 1 is republished from that article here to provide the complete list for polymer properties identified as important to PBF manufacturing. This section provides general background on published research for new high temperature polymer development and briefly highlights the relationships important to high-temperature polymers.

The relationships dominating printing behavior to ensure even powder spreading and a densely packed build piston have been

Table 1

Summary of theoretical material properties for successful PBF printing. * denotes values for nylon-12 for use as “known good,” but should not be regarded as physical limit. Table republished with permission from Elsevier [17].

Powder Recoating

Average particle diameter (d_{50})	45–90 μm
Percentage of fine (< 10 μm) particles	< 5 %
Hausner Ratio	< 1.25
Sphericity	> 0.6
Avalanche Angle	5.25**
Energy Input	
Heat of fusion	90 J/g*
Molecular motion resonance near laser wavelength	10.6 μm
Small temperature range for flow transition:	
Peak width at half max	5 °C*
Difference between onset and endset of melting	10 °C*
Stable molecular weight	EMR _{deg} > > 1 Limited side reactions
Coalescence and Cooling	
Characteristic relaxation time	> > 1
Zero-shear viscosity to surface tension ratio	< 1
Zero-shear viscosity	60 Pa.s*
Surface energy	35–40 mN/m *
Maximum out of plane curl	50 μm *

identified as geometric properties of the powder and not dependent on the chemical identity of the material. The only hint towards a material property relevant to powder flow is that of tribo-charging [27]. High charge concentrations impede powder flow [28], potentially decreasing printed part quality. Although not quantitative, one may conjecture that the greater potential for electron conduction of the aromatic ring structures found in high-temperature polymers will result in quicker dissipation of static surface charge than for aliphatic polymers. This topic is not well studied in the context of polymer PBF.

One other important, although indirect, consideration for polymer-process relationships in high-temperature polymer PBF is the act of powder making. Powder making can be approached either through mechanical size reduction, using methods such as cryo-milling [29], through engineered molten flow instabilities, or else through phase separation techniques, including both immiscible polymer blends [30] and precipitation from small-molecule solvent [31]. The high melting temperatures and general solvent resistance make high-temperature polymers challenging to render into a powdered form.

Of the three sub-functions, the Energy Input sub-function is most important in terms of machine design and process parameter selection for printing high-temperature polymers. Energy Input is comprised of both (i) broad thermal energy provided through resistive or radiative heating elements to heat the entire build chamber above room temperature and (ii) selective optical energy provided by a scanning laser beam. The two sources of energy in PBF are advantageous for printing high-temperature polymers as the total energy needed to melt and fabricate objects is the sum of both sources.

Vasquez, et al. pioneered mapping these two sources of energy in the context of polymer thermal properties via the Energy Melt Ratio (EMR) [32]. The EMR and subsequently developed EMR for degradation (EMR_{deg}) [33] can be used in tandem to generate the Stable Sintering Region (SSR) image to graphically convey theoretically recommended bed temperatures and both the minimum laser power to fully melt the polymer and the maximum laser power before degrading the polymer. Chatham and coauthors altered the original forms of the EMR and EMR_{deg} to incorporate a temperature-dependent specific heat term [34]. The original equations are presented in Eqs. (1 and 3) [33] and their modified forms in Eqs. (2 and 4) [34].

$$EMR = \frac{E_D}{\{C_p \times (T_m - T_b) + h_f\} \times Q \times \Phi} \quad (1)$$

$$EMR = \frac{E_D}{\left[\int_{T_b}^{T_m} C_p(T) \cdot dT + h_f \right] \times (Q)(\varphi)} \quad (2)$$

$$EMR_{deg}$$

$$= \frac{E_D}{[C_p \times (T_m - T_b) + h_f] \times (Q)(\varphi) + [C_p \times (T_{d,1\%} - T_m) + \frac{E_A}{M_w}] \times Q} \quad (3)$$

$$EMR_{deg} = \frac{E_D}{\left[\int_{T_b}^{T_m} C_p(T) \cdot dT + h_f \right] \times (Q)(\varphi) + \left[\int_{T_m}^{T_{d,1\%}} C_p(T) \cdot dT + \frac{E_A}{M_w} \right] \times Q} \quad (4)$$

In the energy melt ratio equation, E_D is energy density, T_m is polymer melting temperature, C_p is specific heat, h_f is the latent heat of fusion, T_b is the bed temperature of the machine, Q is the material density, and φ is the packing ratio of the powder bed. The additional terms of activation energy for degradation (E_A), weight-average molecular weight (M_w), and the temperature at 1% weight loss ($T_{d,1\%}$) are included in the degradation equation.

Although the polymer properties represented in these equations are not specific to high-temperature polymers, the large emphasis on thermal properties means these polymers’ eponymous high melting temperature heavily contributes to printing behavior. What is uniquely important to high-temperature polymers is their deviation from the previously generally accepted rule of “PBF supercooling window” as observed in polyamides. Berretta and coauthors describe this deviation in their publication regarding PBF of PEEK [35]. Separation between melting and cooling behavior as observed by differential scanning calorimetry (DSC) at 10 °C per minute cooling rate was previously regarded as essential behavior for a polymer to be regarded as printable [36]; however, no high-temperature polymer reported in PBF literature demonstrates this behavior and yet, dimensionally accurate parts have been fabricated using these materials. This disparity between high-temperature polymers and engineering grade polymers has not yet been thoroughly investigated; however, the answer is likely related to rate of crystallization [37].

It is important to note that the existing screening methods for polymer PBF assume the polymer exhibits a semi-crystalline morphology. Amorphous polymers are rarely reported in PBF literature. The latent heat of melting required to melt crystalline regions is beneficial for ensuring selectivity of melt-pool formation when printing [38]. A well-defined melt-pool shape is more difficult to maintain for an amorphous polymer where the temperature gradient induced by the scanning laser would result in a degree of flow behavior in the powder bed immediately surrounding the scanned area. This could lead to significant part growth in the XY plane as well as significant porosity in this region resulting from partial coalescence of powders in the transition region. Stable crystalline regions restrict flow in the regions immediately adjacent to the scanned area of the powder bed, thereby maintaining selectivity of fusion and dimensional accuracy. Bain reports melting behavior in many high-temperature polymers occurs over a wide temperature range [37]. Some researchers recommend using the ratio of specific heat and heat of fusion (C_p/h_f) to represent the gradual transition from glass to melt [39]. Polymers with lower ratios can be heated closer to T_m without a thermal gradient causing undesired fusion. This allows the onus of melting to be placed on the heaters instead of the laser beam [39]. Lyons suggests the higher ratio of the high-temperature PAEK family compared against the polyamide family indicates a more gradual transition into the melt for PAEKs. Both factors of broad T_m and higher C_p/h_f indicate high-temperature polymers are more sensitive to thermal gradients than polyamides (PAs) [37]. Lyons also highlights the nearly two times greater specific heat of PAEKs over PAs (2.20 vs 1.26 $\text{J g}^{-1} \text{K}^{-1}$) means nearly twice as much energy must

be expended per each degree to heat high-temperature polymers [39].

The polymer-process interactions during the third PBF sub-function (i.e., Coalescence and Cooling) is best represented by the Deborah number (De) for coalescence, shown in Eq. 5 where λ is the characteristic relaxation time (i.e., longest) of the polymer, Γ is surface tension, η_0 is zero-shear melt viscosity, and a_0 is average particle size.

$$De = \frac{\lambda \Gamma}{\eta_0 a_0} \quad (5)$$

The high T_g characteristic of high-temperature polymers implies that similarly high temperatures are required to reduce viscosity to a value allowing chain mobility on the timescale of manufacturing. Particle coalescence is governed by extensional flow, therefore either the extensional viscosity or steady-shear viscosity and the Trouton ratio should be used. In addition, proper viscosity must be maintained over a minimum period of time to achieve coalesced layers. According to a patent issued to the polymer company Arkema, a polymer should have a steady-shear viscosity at shear rates below 5 rad s^{-1} between 800 and 20,000 Pa.s for at least 5 min to be suitable for PBF [40]. This range is higher than the 60 Pa.s reported by Shi, et al. [41] as the ideal viscosity calculated from applying nylon 12 properties to Frenkel's model for viscous sintering [42].

High-temperature engineering polymers generally have high values for zero-shear viscosity. This directly translates into a processing challenge as viscosity opposes coalescence. Exploiting the typical inverse relationship between polymer viscosity and temperature necessitates high processing temperatures to drive coalescence. Conversely, high surface energy and long characteristic relaxation times increase the coalescence rate. Surface tension is chemistry dependent, but no general trends have been observed for changing surface tension with the inclusion of aromatic rings in polymer backbones. However, the additional molecular level stiffness imparted to polymer chains by aromaticity increases the characteristic relaxation time through an increase in Kuhn length (i.e., $\lambda \sim b^2$). Therefore, high temperature engineering polymers would be expected to have a longer characteristic relaxation times when compared to other classes of polymers with more flexible backbones. The ultimate question for high-temperature polymer coalescence is at what temperature can the driving forces of relaxation time and surface tension overcome dissipative losses imposed by high zero-shear viscosity.

3.2. Material extrusion: process

The major constituents of a typical MatEx system are the feed material, liquefier, print nozzle, gantry, print bed, and print chamber [43]. The quality of print is affected by different process parameters such as print temperature, layer height, air gap, and raster angle [44]. MatEx uses polymer material feed either in the form of pellets (e.g. pellet extruders from Titan Robotics [45] and Strangpresse [46]) or filament (fused filament fabrication), which is fed into a printing head using a pinch roller mechanism. The feed in the printing head is then heated, liquefied, and extruded through a nozzle. Usually a thermocouple is used in addition to the heating element and a controller to maintain the set print temperature [47]. The feed velocity (v_f) required to obtain a layer of width w and thickness h is given by Eq. (6) [43]:

$$v_f = \frac{V}{w \cdot h} \quad (6)$$

where, V is the volumetric flow rate of the polymer melt through the nozzle. The power (P) required by the motor to extrude a filament having a cross-section area A is given by the following equation:

$$P_M = \frac{1}{2} v_f A (\Delta P) \quad (7)$$

where, ΔP is the pressure drop across the nozzle which can be

calculated from the polymer melt viscosity, flow rate, and geometric constants of the nozzle. It should be kept in mind that in the melt state, the properties depend on both temperature and shear rate and can be a bit complicated to compute [48]. Another important design consideration is the maximum viscosity of polymer melt that a MatEx printer can handle without issues such as nozzle clogging and filament breakage. The maximum viscosity that a MatEx printer can handle depends on the capacity of the extrusion motor. If F is the force required to drive a filament with radius R_f through a nozzle of length L and radius R_N then the maximum viscosity (η) is given by Eq. (8) [49] as shown below:

$$\eta = \frac{F \times R_N^4}{8 \times V \times R_f^2 \times L} \quad (8)$$

High temperature engineering thermoplastics generally have an aromatic backbone which imparts higher molecular stiffness and reduced chain mobility to the polymers when compared to thermoplastics having an aliphatic backbone (e.g., nylon, polyolefins, etc.). Thus at comparable molecular weights, the engineering thermoplastics typically require higher temperatures for processing. At comparable temperatures, the values of η_0 for the engineering polymers are significantly higher than that of linear chain polymers which present significant processing challenges in MatEx. Therefore, these polymers should be printed at shear rates where they exhibit shear-thinning behavior. Polymers having a limited shear-thinning window have been found to suffer from backflow during MatEx printing [50]. Increasing the print temperature can assist printing by lowering the melt viscosity and also increasing the time a deposited layer stays above T_g , thereby improving the weld strength. Injection molding grade polymers have considerably higher melt viscosities than MatEx grade filaments [51]. In order to further ease processing, plasticizers can be incorporated to the pure polymer to lower the melt viscosity but they can have an adverse effect on the tensile strength and modulus [52]. Blending such plasticizers can improve the quality of the printed part at the expense of reducing the form-stability.

After being extruded out of the nozzle, the extruded material is deposited onto a print bed in a 2-dimensional pattern, where it cools below its crystallization temperature and/or T_g and solidifies. The print bed and heated chamber are important elements in a MatEx system designed for high temperature thermoplastics. The polymer melt must have sufficient adhesion after deposition so that the build can continue without delamination. Further, in order to minimize residual stress buildup, the polymer should have minimum CTE mismatch and melt shrinkage. However, the adhesion between the deposited layer and the bed should not be too strong, otherwise part removal after completion of the print becomes complicated. This issue is exacerbated for high temperature polymers since the driving force for delamination (i.e., the difference between print temperature and bed temperature) is higher than for other standard plastics because of increased thermal gradients and CTE mismatch. The interactions among the process controls, material systems, process parameters and printed part property have been reviewed in great detail in previous reported literature [43,53,54]. Also, the role of rheology in MatEx has been reviewed elsewhere [55]. In this review paper, we investigate the high temperature polymers that can be processed using MatEx, evaluate what makes them "printable", the process and machine modifications required for successful printing, and the associated current limitations.

4. High temperature engineering thermoplastics in additive manufacturing: Structure

With the advancement in polymer chemistry and material synthesis over the last 50 years, novel materials are being regularly formulated and tested with respect to their printability and compatibility with AM. Based on the operating temperatures and physical nature, they are

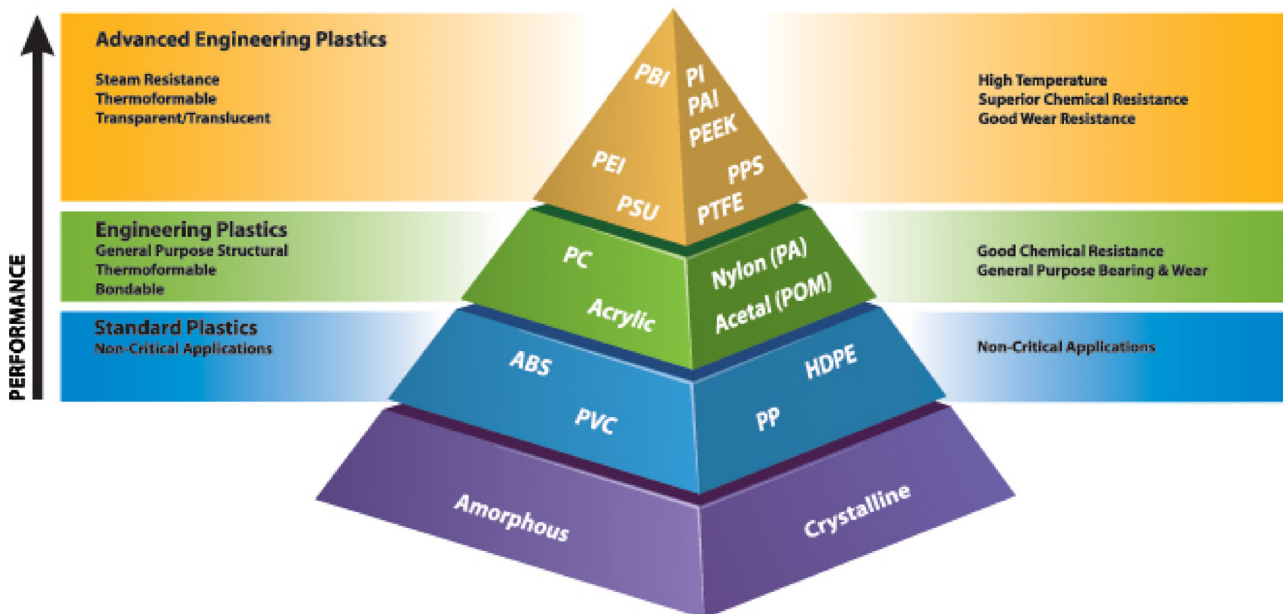


Fig. 1. Overview of high temperature thermoplastics as a function of performance (image reproduced from [56]). Although performance increases as we go up in the pyramid, the difficulty of processing and associated costs increases rapidly.

classified as advanced engineering plastics, engineering plastics and standard plastics, as illustrated in Fig. 1. Many of the standard plastics are commercially available and can be used off-the-shelf as a feedstock for AM but processing engineering plastics by AM is still in the nascent stage.

Fig. 2 highlights the polymer backbone (repeat units) of some common high-temperature thermoplastics that are printed using MatEx and PBF modes of AM. It is worth noting the aromatic backbone common to these polymers. This featured moiety increases molecular-level stiffness and introduces secondary interactions, like π - π stacking, that increase the energetic threshold for molecular motion; i.e., temperature required for flow. This section introduces the material types and properties of high temperature engineering thermoplastics that are currently being used in MatEx and PBF as listed in Table 2. The data tabulated in Table 2 also serves as a basis for comparison of mechanical properties of the high temperature engineering thermoplastics processed using traditional manufacturing techniques (typically, injection molding) versus properties obtained by MatEx and PBF modes of manufacturing (highlighted in Tables 3 and 4).

4.1. Overview of high temperature engineering thermoplastics in PBF

In this section, the authors present a summary of high-temperature polymers printed via PBF. Table 3 summarizes the print parameters and resultant mechanical properties as reported in published literature. The quantity of total published research in the field of polymer PBF is less

than that of MatEx; therefore, the sub-set of published work pertaining to high-temperature thermoplastics scales reasonably. Most of the published work centers on poly(ether ketone) (PEK) and poly(ether ether ketone) (PEEK), both members of the poly(aryl ether ketone) family. There are a few published research documents which investigate printing poly(phenylene sulfide) (PPS) alongside reports of a commercial “PBF-grade” PPS powder by Toray [80]. Fig. 3 highlights the tensile strength of some high temperature engineering thermoplastics manufactured using PBF.

There is also an absence in published literature regarding any chemical synthesis or modification strategies of high-temperature polymers that would specifically render them PBF printable. Likewise, any literature discussing including additives in high-temperature polymers for PBF is strictly concerning final part modification of mechanical properties, and not acting as a processing aid. This is a current gap in published literature, therefore, the discussion in this section will focus on the process parameter value selection and the resultant mechanical properties of PBF printed high-temperature thermoplastic polymers. A discussion of machine specific concerns will follow in Section 6.

A significant gap in current literature revolves around consensus of dissemination of important print parameter values to enable fundamental interpretation and implementation of published results for further research. This is evidenced by the quantity of empty spaces in Table 3. For equitable comparison and understanding, the authors believe that, at minimum, each publication should report all variables present in the energy density equation (i.e., laser power, beam speed,

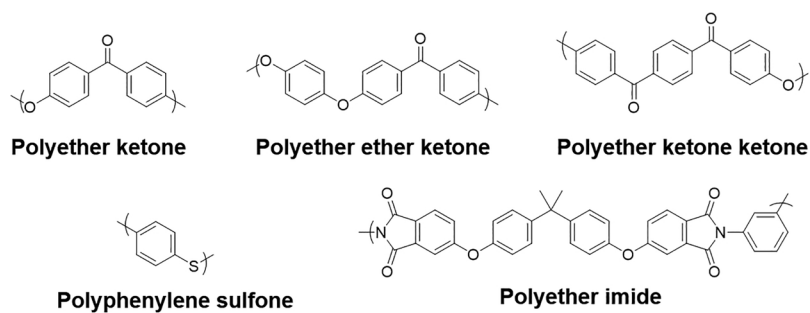


Fig. 2. Repeat units of common high temperature engineering thermoplastics used in AM.

Table 2
Overview of properties of high temperature thermoplastics as obtained using traditional processing techniques, typically injection molding.

Polymer	Service temperature (°C)	T _m (°C)	T _g (°C)	Mechanical properties	General characteristics	Traditional applications
Poly ether ketone (PEK)	260 [57]	373 [58]	162 [58]	4.0 GPa tensile modulus; 105 MPa tensile strength, and 15 % ultimate strain [59]	Excellent mechanical properties; high thermal stability; chemical resistance. High strength at elevated temperatures; low moisture uptake.	Structural parts with high load bearing capacity; personalized implants
Poly ether ketone ketone (PEKK)	125–204	390 [60]	156 [61]	4.20 ± 0.81 GPa tensile modulus; 102.0 ± 3.9 MPa tensile strength, and 62.1 ± 2.5 % ultimate strain [62]	Resistant to mechanical wear, creep deformation, and chemical degradation.	Aerospace industries; surgical implants [63].
Poly ether ether ketone (PEEK)	204–232 [64]	343 [65]	143 [65]	1.28–4.10 GPa tensile modulus; 92.3 MPa tensile strength, and 40 % ultimate strain [66,67]	Chemically resistant; wear resistant; electrically conductive [72]	Automotive, aerospace, textile industries; and medical implants.
Poly phenylene sulfide (PPS)	204–232 [64]	285 [68]	85 [69]	3.697 GPa tensile modulus; 64–82 MPa tensile strength, 3% ultimate strain [70,71]	High strength & stiffness; recyclable; fire retardant, creep resistant [75–79]	Automotive, aerospace, electrical, electronics.
Poly ether imide (PEI)	177–204 [64]	330–380 (amorphous)	217 [73]	2.934 GPa tensile modulus; 102.5 MPa tensile strength; 18 % ultimate strain [74]		Aircraft interiors, automotive, and marine industries.

hatch spacing, and spot size) and the bed temperature. Other important material or powder properties to include are found in the EMR equation given by Vasquez, et al. [32] and previously discussed in Section 3.1. These polymer properties should also be evaluated at the processing temperature, and not at room temperature. Quantification of properties, like specific heat, often significantly change upon heating the polymer from the glassy state through the glass-transition temperature and towards melting. Considering and reporting relevant properties is important for accurate process parameter value prediction.

4.2. Overview of high temperature engineering thermoplastics in MatEx

The material catalog for MatEx has long been an issue in advancing the application of this technique to the industrial market. Materials for MatEx are often limited by the rapid cooling rates (arising from the large difference between the print and ambient temperature), phase transformation, and separation. Common commercial materials are limited to polylactic acid (PLA) and acrylonitrile butadiene styrene (ABS), which both become fluidic at temperatures less than 250 °C [94–96] and have a tensile strength less than 60 MPa [97,98]. While these polymers are suitable for prototyping, they do not possess the strength or other enhanced-value properties needed to manufacture functional parts. This is especially true for the AM early-adapter industries of automotive, aerospace, and biomedical, which require parts to survive in extreme environments. A deeper understanding of the structure-property-processing relationships between polymers and the MatEx process is needed to expand the material catalog to rival the options available for traditional manufacturing technologies.

By the definition of “high temperature thermoplastics” discussed previously in this review, the available high-temperature polymers for MatEx include: polyether ketone (PEK), polyether ether ketone (PEEK), polyether ketone ketone (PEKK), polyphenylene sulfide (PPS) and polyether imide (PEI). Fig. 4 highlights the tensile strengths of different high temperature thermoplastics and their composites printed using PBF and MatEx. As evident from Fig. 4, the properties can be quite different even for the same material depending on the formulation, grades, reinforcement agents, and print conditions. Table 4 summarizes the printing conditions and corresponding mechanical properties obtained by printing high temperature engineering thermoplastics using MatEx.

Many high temperature engineering thermoplastics are semi-crystalline; the advantages of using semi-crystalline polymers over commercially available amorphous materials are improved thermal stability, toughness and deformability [99,100]. The introduction of crystallites acts as physical crosslinks that restrict the motion of the polymer chains, even above the T_g, which allows semi-crystalline materials to be used for longer times at higher temperatures without loss of mechanical properties. However, incorporating semi-crystalline high temperature materials in MatEx is challenging due to shrinkage of the printed parts as it cools and crystallizes inside a heated chamber on the printer bed [101]. The aforementioned crystallites are one of the primary reasons that these materials are not often used in MatEx. Due to high levels of shrinkage the parts fabricated using this technique tend to warp and delaminate from the printer bed resulting in parts of poor quality that are unfit to be used in high performance applications as illustrated in Fig. 5. The shrinkage occurring in these materials is more pronounced as compared to the amorphous polymers due to increased densification in semi-crystalline materials during the crystallization process [102].

Crystallinity also has a significant effect on the interlayer bonding, which is vital to the success of MatEx. Boiko, et al. showed that interlayer bonding is greatly hindered by crystallinity in the polymer matrix as a result of the crystals acting as barriers to polymer chain diffusion [103]. They demonstrated that the bond strength formed between two semi-crystalline materials is an order of magnitude lower than that between two amorphous materials, or even between an amorphous and

Table 3

Summary of mechanical properties of PBF printed high-temperature thermoplastic polymers.

Polymer	Bed temperature (°C)	Laser power (W)	Beam speed (mm s ⁻¹)	Ultimate tensile strength (MPa)	Ultimate tensile strain (%)	Other	Reference
PEKK				50		3.3 GPa modulus	[81]
PEK						3.5 GPa modulus	[82]
PEK (HP3)	368			90	3–4		[83]
PEK (HP3)	365		2550	88 ± 7			[84]
PEK (HP3)				90	2.8	4.25 GPa modulus	[85]
PEEK	200	10	1530	79 ± 3		560 μm spot size	[86]
PEEK Victrex 450 PF	332	7.5–16.5	2550	31–37			[87]
PEEK Victrex 150PF	338			41		2.5 GPa modulus	[87]
PEEK Victrex 150XF	140	16–21	5080			Porous structure	[88]
EOS PEEK HP3				88.7 ± 1.5	4.2 ± 0.2	2.76 ± 0.15 GPa modulus	[89]
PEEK + Carbon fiber (CF)		11–18.5	3000	109 ± 1		0.5 GPa modulus	[90]
PEEK + Carbon Black (CB)	330		2500–6000	30–50		Nd:YAG laser	[91]
PPS	200	11	1000	64.5			[92]
PPS	230	30	3000	61.8 ± 4	3.27 ± 0.22	2.44 ± 0.04 GPa modulus	[34]
PEI	Room Temperature	60–67.5	2000	15–37	3–5.7	737–1321 MPa modulus	[93]

a semi-crystalline material. These results are corroborated by similar studies conducted by Cho and Kardos [104] and Awaja, et al. [105]. However, crystallization after bonding produced a bond strength even greater than that between the two amorphous materials. This is due to a process called co-crystallization, which is the process of a crystallite growing across a bonded surface, thus holding the two adjacent layers together [106–108].

5. Processing high temperature engineering thermoplastics: Properties

This section highlights the recent progress made in printing high temperature engineering thermoplastics using both PBF and MatEx modes of AM. Our discussion is limited to the commonly used engineering thermoplastics such as PEK, PEKK, PEEK, PPS, and PEI. The current state of the specific materials with respect to printing are analyzed along with the limitations associated and research gaps.

5.1. Polyether ketone (PEK)

5.1.1. PBF

HP3, sold by EOS for use with their P800 machine, is commercially available as a “PBF-grade” PEK [85]. Although advertised as “HP3 PEEK,” Ghita and coauthors assert that EOS HP3 is chemically PEK with a peak melting temperature of 372 °C [83]. With this elevated melting temperature, they report printing HP3 PEK at 368 °C using an EOS P800 [83]. Although hot stage microscopy shows full particle coalescence with new powder, they report reduced coalescence at the same temperature with used or blended (a.k.a., “refreshed”) powder. The longevity of PBF powder is an important concern, especially for high-temperature polymers, due to their high raw material cost. Ghita and coauthors purport that holding PEK at these elevated processing temperatures for extended periods of time results in branching and cross-linking [136] which adversely affects coalescence behavior during printing [83]. Berretta and coauthors report in greater detail on the coalescence and fusion behavior of PBF PEK concluding that the faster coalescence from lower viscosity PEK produces denser parts that are also weaker under tensile loading [84]. Their explanation is that although the lower molecular weight PEK results in a lower viscosity, which promotes particle fusion, the lower molecular weight polymer is intrinsically weaker on the molecular scale [84]. Recently, PBF of carbon fiber encapsulated HP3 PEK powders has been performed and the powder properties has been optimized with respect to the printing

process [137].

5.1.2. MatEx

There are not many published works of research that look into the potential of printing PEK by MatEx. However, most of the work done on PEKK at the Oak Ridge National Laboratory should be helpful in enhancing the understanding of MatEx based printing of PEK. The researchers have investigated how the melt processing of the high temperature semi-crystalline polymers and subsequent post-processing affect the rheological properties of fiber reinforced polymer matrices which are relevant to MatEx as well as big area additive manufacturing (BAAM) [138–142]. Their work will be discussed in greater detail in the next section, which focuses on PEKK.

5.2. Polyether ketone ketone (PEKK)

5.2.1. PBF

PBF printed PEKK is, perhaps, the most industrially used high-temperature polymer [143–145]. In addition to strength at elevated temperatures, commercial PBF grades of PEKK are flame retardant [39] and can be used in applications requiring electrostatic discharge [146].

PBF printing of PEKK is reported by Peyre and coauthors [147] and their relevant doctoral theses [60,81]. Peyre, et al. printed PEKK using a custom machine able to reach at least 325 °C. These researchers note the diminished “PBF supercooling window” of PEKK in comparison with nylon 12. They also remark on the significant geometric distortion during printing. They do not report mechanical properties of printed parts as the main focus of their project emphasizes the agreement between numerical simulation of warping and experimentation of PBF printing. A more recent study on PEKK investigated the effect of material properties on printed part shrinkage during PBF [148]. The results suggest that the inherent powder properties (particle size, distribution, morphology, porosity) have a more pronounced effect compared to crystallization on the extent of part shrinkage. As such, the Kepstan 6000 PEKK used in the study was found to have 30 % lower shrinkage compared to nylon [148].

Bain discusses the relative advantages of PEKK over other high-temperature polymers in a summary of polymers in PBF [37]. A high T_g , slower crystallization kinetics [149] and lower T_m , and therefore printing temperature, than PEEK and PEK are realized as economic benefits through reduced energy cost. Additional economic benefit is realized through the recyclability (i.e., reuse of un-fused powder in subsequent builds) of PEKK, which is observed to be significantly

Table 4
Summary of mechanical properties of MatEx printed high-temperature thermoplastic polymers.

Polymer	Tensile strength (MPa)	Tensile modulus (GPa)	Print conditions	Reference
PEEK pellets (450 G Victrex) PEEK powder (Victrex 450 PF)	84 98.9 ± 2.3	4 3.98 ± 0.78	Nozzle temperature of 420 °C; ambient temperature of 150 °C, 0° raster angle Nozzle temperature of 400 °C; bed temperature of 100 °C; ± 45° raster angle; 0.2 mm layer height; 20 mm/s speed; 100 % infill	[109] [110]
PEEK PEEK (Luvocomm, Germany) PEEK (Arevo Labs) PEEK filament (Apium PEEK 450 Natural)	56 69.04 ± 7.01 74.49 84 ± 5.9	3.53 ± 0.01 2.8 3.33 ± 0.01	0°/90° raster angle; 300 µm layer thickness Nozzle temperature of 420 °C; bed temperature of 110 °C; 75 % infill; 20 mm/s speed; 0.1 mm layer height Nozzle temperature of 340 °C; bed temperature of 230 °C; 50 mm/s speed; 1.00 % infill; 0.25 mm layer height Nozzle diameter 0.4 mm; nozzle temperature 400 °C; bed temperature 100 °C; 20 mm/s speed; 0.1 mm layer height; ± 45° raster angle; 100 % infill	[111] [112] [113] [114]
PEEK filaments Victrex® PEEK 450 G filaments Victrex® PEEK 450 G PEEK 450 G filaments Victrex® PEEK 450 G + Carbon nanotube (CNT)	40.0 ± 4.4 75.06 82.58 ± 1.03 76 87.7 ± 7.0	0.52 ± 0.03 3.80 ± 0.03	Nozzle temperature of 370 °C; 60 mm/s speed; 0.2 mm layer height; 40 % infill Nozzle temperature of 420 °C; ambient temperature of 80 °C; bed temperature of 130 °C; 100 % infill; ± 45° raster angle Nozzle temperature of 410 °C; bed temperature of 100 °C; 100 % infill; 0.1 mm layer height Nozzle diameter of 0.4 mm; nozzle temperature of 440 °C; 0.1 mm layer height; 20 mm/s speed Nozzle temperature of 365 °C; 0.2 mm layer height; 30 mm/s speed	[115] [116] [117] [65] [118]
PEEK (450 G, Victrex) + 1% CNT PEEK (450 G, Victrex) + 5% CF PEEK pellets (450 G, Victrex) + 5% CF PEEK pellets (3DX tech) PEEK + 5 wt% GNP PEEK + 3 wt% CNT PEEK (VESTAKEEP 3300 G)	66 72 72 101.41 ± 4.23 300.1 66.2 ± 2.61 58.5 ± 3.06 63.4 ± 1.02 96.90 ± 1.87	3.79 ± 0.27 7.37 ± 1.22 5.1 3.15 ± 0.11 3.89 ± 0.15 3.77 ± 0.04 3.54 ± 0.67	Nozzle temperature 420 °C; ambient temperature 20 °C; 0.2 mm layer height; 40 mm/s speed; post printing parts were tempered at 300 °C for 2 h Nozzle temperature 390 °C; bed temperature 100 °C; 1000 mm/min speed; 0.48 mm extrusion width; 100 % infill; 0.1 mm layer height Nozzle temperature 390 °C; bed temperature 100 °C; 30 mm/s speed; 0.15 mm layer thickness; 0/15°/−15 raster angle; 0.4 mm line width 100% infill; post printing parts were annealed at 250 °C for 2 h Nozzle temperature of 375 °C; ± 45° raster angle Nozzle temperature of 420 °C; 0° raster angle Nozzle temperature of 335 °C; bed temperature of 165 °C; ± 45° raster angle; 0.1 mm layer height; 50 mm/s speed; 100 % infill	[120] [121] [122] [123]
PEI Ultem 9085 PEI Ultem 1000 + 10 wt% CF PEI Ultem 1000 + 1 wt% Carbon nanofiber (CNF)	62 ± 0.1 50 ± 0.9 97.6 ± 4.6	2.23 ± 0.012 2.9 ± 0.048 1.69 ± 0.039	Nozzle temperature 300 °C; bed temperature 100 °C; ambient temperature 30 °C; 30 mm/s speed; 0.15 mm layer thickness; 0/15°/−15 raster angle; 0.4 mm line width 100% infill; post printing parts were annealed at 250 °C for 2 h Nozzle temperature of 375 °C; ± 45° raster angle Nozzle temperature of 420 °C; 0° raster angle Nozzle temperature of 335 °C; bed temperature of 165 °C; ± 45° raster angle; 0.1 mm layer height; 50 mm/s speed; 100 % infill	[124] [125]
PEI Ultem 9085 PEI Ultem 9085 PEI Ultem 9085 PEI Ultem 1010 PEI Ultem 1010 + CNT PEI + 20 % CF PPS + 40 % glass fiber (GF)	72.6 71.0 ± 2.6 89.0 ± 1.2 98.40 ± 8.0 125.3 ± 4.5 61.1 51.2 61.9 ± 2.0 74.03 ± 1.65 57.3	2.48 ± 0.19 ~3.0	254 µm layer thickness; post printing parts were treated with chloroform for 2 h 254 µm layer thickness; other parameters optimized based on software input data Nozzle temperature of 385 °C; environment temperature 170–190 °C; 254 µm layer thickness, 0° raster angle Nozzle temperature of 375 °C; bed temperature of 162 °C Deposition temperature of 364 °C; retrofit extrusion screw; deposition rate of 4.5 kg/h Deposition temperature of 357 °C; Dohle extrusion screw; deposition rate of 4.5 kg/h Nozzle temperature of 310 °C; 15 mm/s speed; 0.2 mm layer height; 90° raster angle; 100 % infill Nozzle temperature of 365–382 °C; bed temperature of 110 °C; 254–279.4 mm/s speed Nozzle temperature of 385 °C; air temperature 27 °C; relative humidity of 60 %; ± 45° raster angle; 0.3 mm layer height; 680 mm/min speed	[126] [127] [128] [129] [130] [131] [132] [133]
PPS + CF PPS PPS + 67 % thermotropic liquid crystalline polymer (TLCP)	93.2 ± 11.27 45.0 ± 6.0 108.5 ± 19.4	26.38 ± 1.18 3.5 ± 0.6 25.9 ± 1.1	Nozzle temperature of 321 °C; bed temperature of 240 °C; 200 in. min speed Nozzle temperature of 300 °C; 1200 mm/min speed; 0.5 mm layer height; 0.6 mm layer width; 0° raster angle Nozzle temperature of 300 °C; 1200 mm/min speed; 0.5 mm layer height; 0.6 mm layer width; 0° raster angle	[134] [135]

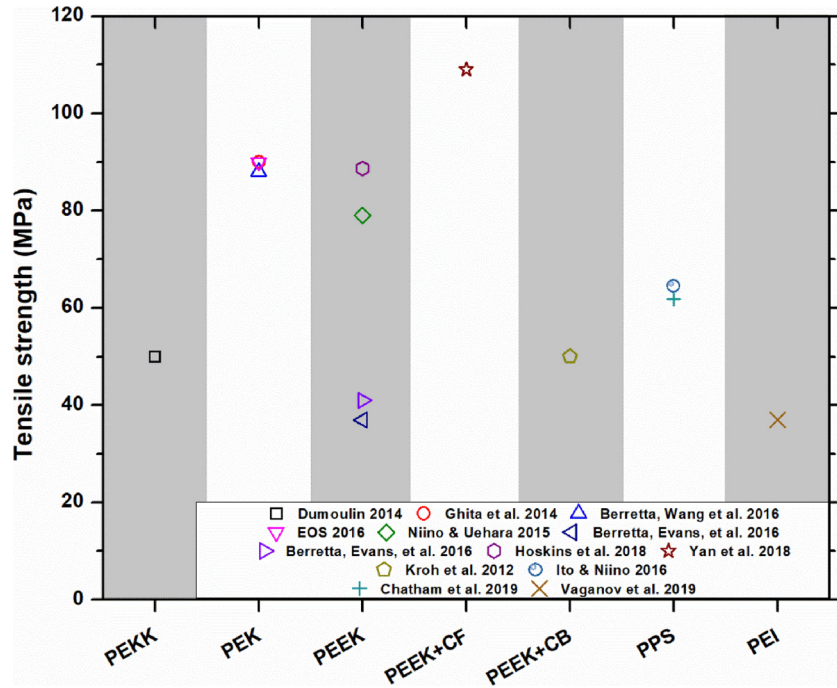


Fig. 3. Tensile strength of high temperature thermoplastics and their composites printed using PBF.

increased over the HP3 PEK material [146]. In fact, Fischer, et al. report only a slight decrease in tensile strength of ALM's CF/PEKK using a refresh rate of 50 % [150]. This value is at the high end of refresh rates reported for nylon-12 [151], thus contributing to PEKK's industrial relevance and importance.

Above its other properties, PEKK's high degree of powder reuse motivates the push for industrial adoption [152]. Unlike many other high-temperature polymers, PEKK has been observed to maintain consistent rheological properties over the course of multiple builds. Once-reused PEKK was validated to meet the stringent, aerospace product quality specifications as part of the America Makes project [152]. The

exact chemical identity of the Oxford Performance Materials PEKK used is not explicit in the report; however, its reusability indicates it is likely to be a copolymer such as the ones discussed by Bain [37].

5.2.2. MatEx

Initial work with PEKK involved studying the flow behavior of the PEKK melt over different temperature ranges to establish an optimum processing window [138]. The authors analyzed the effect of MatEx based processing on semi-crystalline engineering thermoplastics as well as their composites with carbon fibers (CF) using a custom-built desktop printer. Their results suggested that the processing temperatures played

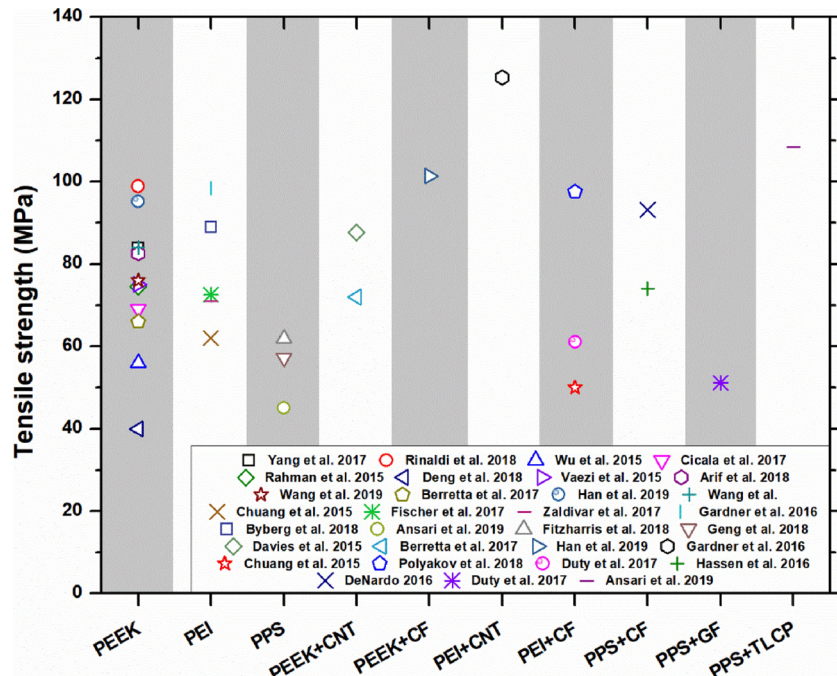


Fig. 4. Tensile strength of high temperature thermoplastics and their composites printed using MatEx.

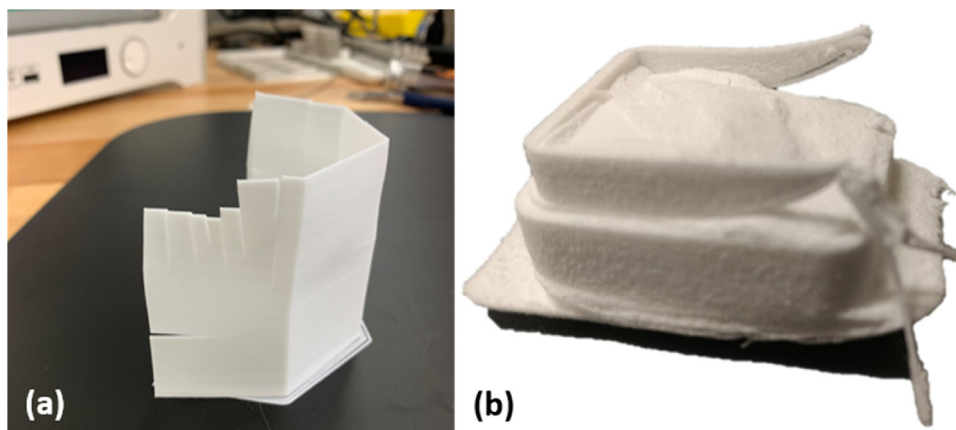


Fig. 5. Challenges associated with printing materials using MatEx (a) poor interlayer adhesion and (b) part delamination occurring during the print.

a crucial role in determining the weld strength of the interfacial bonds. Moreover, rheological analysis suggested that there exists a correlation between the changes occurring at the molecular level and the bulk strength of the bonds formed during the printing process. Another important conclusion drawn from this study was that the temperature at which the semi-crystalline materials are processed dictates the bond strength of the rasters during the print [138].

Subsequent work from the same research group dealt with further in-depth analysis of the rheology of the PEKK samples with special focus on processing in MatEx [139]. Depending on the processing parameters like temperature, shear rate and filler material, they developed a screening process based on rheology of the polymer to optimize the parameters that can then be used in successfully printing functional parts via MatEx. Similar work based on rheological analysis was performed on PEKK and its composites with CFs to identify proper processing conditions in MatEx with the ultimate goal of evaluating the suitability of these materials in BAAM [140]. However, the viscosity decreased only by 4–6 % upon increasing the temperature from 375 °C to 390 °C. The high viscosity of the PEKK/CF composites at relevant shear rates ($\sim 100 \text{ rad s}^{-1}$) resulted in a pressure drop higher than what the BAAM system could handle and hence printing failed.

5.3. Polyether ether ketone (PEEK)

5.3.1. PBF

PEEK is often processed at around 360 °C and used in high temperature applications [75]. Moreover, the modulus of PEEK remains largely unaffected for brief intervals even at temperatures higher than its T_g (143 °C) which broadens its application window [111]. PEEK begins to show up in the PBF literature in the early 2000s; however, at this stage, it was as “coating grade” or “injection molding grade” PEEK and not as a PBF optimized grade of PEEK like companies now offer. The exact compounding modifications are unknown. Much of the literature involving PBF printed PEEK focuses on biomedical applications [88,153,154]. The published body of work is therefore more focused on aspects of the printed parts, like cell viability and dimensional accuracy, than on how PEEK interacts with the manufacturing process itself.

Tan and coauthors blended hydroxyapatite with a coatings grade Victrex PEEK™ 150XF powder to fabricate implantable cell-scaffolds for tissue engineering. These powders fell below the recommended average particle size of 45–90 μm [16] with an average particle size of 25 μm [88]. Contrary to current methods for printing high-temperature polymers, Tan and coauthors used a bed temperature of only 140 °C [88,153] instead of something closer to the 350 °C melting temperature of PEEK. Similarly, Niino and coauthors reports printing PEEK at 200 °C, but with a modified laser beam profile for a more efficient use of optical energy in fabrication [86]. One of the advantages to printing

cell scaffolds is that cell scaffolds should have high porosity, and therefore it is unnecessary to produce fully dense parts.

When final part density is an important metric, a higher bed temperature will be more important. Schmidt, et al. report achieving above 90 % relative density of PBF printed PEEK and identify the trend of higher bed temperature resulting in more dense parts [155]. These researchers recommended printing at higher bed temperatures to avoid degradation caused by excessive laser power [155]. Rechtenwald and coauthors concluded from their statistical design of experiments that bed temperature is the most influential parameter of the four parameters investigated (temperature, laser power, beam speed, hatch spacing) [156]. An interesting note is that while temperature represents thermal energy input, the other three factors represent optical energy input, implying greater importance of thermal energy. The field of high-temperature polymer PBF would greatly benefit from a statistical design of experiments study comparing the effects of total thermal energy input with total optical energy input. It should also be noted that the maximum bed temperature in the Rechtenwald study was 250 °C [156]. It is possible that a different trend regime exists in a temperature range closer to the melting temperature of the polymer.

In addition to neat PEEK, research groups led by Chen [157] and Yan [90] have reported printing reinforced PEEK composites. Chen and coauthors added graphene nanocomposites to PEEK powder through both wet and dry mixing. They report improvement in both mechanical properties and electrical conductivity of resultant parts [157]. Yan and coauthors incorporated CF into PEEK powder and report ultimate tensile strength as higher than injection molded, neat PEEK. Their $109 \text{ MPa} \pm 1 \text{ MPa}$ ultimate tensile strength and $7.4 \pm 0.5 \text{ GPa}$ modulus is measured despite hindrance to particle coalescence resulting from including CF [90].

5.3.2. MatEx

The first reported literature on printing PEEK by MatEx was published by Valantan et al. [158] who designed and developed a modified desktop MatEx machine, which was able to print with two different commercially available grades of PEEK-Optima®. Although their results showed a significant drop in the mechanical strength of the printed parts as compared with parts made using traditional molding techniques, they postulated that with additional testing PEEK printed using the custom-made machine can be used to manufacture bone replacement implants due to its excellent mechanical properties and biocompatibility. Studies on other biomedical applications (such as, dentistry) of 3D printed PEEK has been summarized in an excellent review article elsewhere [159].

The challenges of fabricating PEEK parts for biomedical applications using MatEx due to the high viscosity of the melt have been reported in a more recent literature [116]. Using the same grade of PEEK as used by

Valentan et al., Vaezi and Yang [116] designed another MatEx machine that could successfully print PEEK samples. They optimized the processing parameters with respect to the tensile and flexural properties of the printed parts and reported an extruder head temperature of 400–430 °C, a print environment temperature of 80 °C and a printer bed temperature up to 130 °C to be the ideal printing conditions for their samples. Parts printed with 100 % infill had superior tensile strength compared to those printed with 80 % infill due to an increase in porosity.

Wu et al. [160] studied the effect of print environment and extruder head temperature on the warping and delamination of PEEK parts printed using MatEx and found that at higher temperatures warping was reduced due to the slower stress relaxation. Subsequent work from the same group [111] investigated the effect of different layer thicknesses (namely, 200, 300 and 400 µm) and different raster angles (namely, 0°/90°, 30°/-60° and 45°/-45°) on the tensile, compressive and bending properties of PEEK printed using a custom-built MatEx system. The samples printed with a 0°/90° raster angle with a layer thickness of 300 µm (higher layer thickness resulted in dimensional instability due to weak interfacial bonding) had the maximum tensile strength (56.6 MPa) as the filaments were oriented parallel to the direction of the load in this configuration.

The effect of raster angle on the mechanical properties of PEEK printed using MatEx was investigated by Cicala et al. [112]. Although the printed PEEK was mechanically superior to other state of the art materials tested in the study there still remained areas for improvement and further research was recommended to reduce the formation of pores during the printing process which negatively affected the mechanical properties of the printed parts. The effect of build environment temperature, extruder head temperature and post processing treatments on mechanical properties of PEEK printed using MatEx was studied by Yang et al. [109]. The results suggested that the PEEK parts printed at 0° raster angle had greater crystallinity and mechanical strength as well as stiffness when processed at increased temperatures (environment and nozzle) and annealed for a longer period of time at higher temperatures.

Rahman, et al. successfully printed PEEK using MatEx and investigated the effect of raster angle on the mechanical properties [113]. This group showed that 0° raster orientation, or all roads oriented in the longest direction of the print, had the greatest ultimate tensile stress, ultimate compressive strength, ultimate flexural strength, and impact energy. The researchers used a proprietary PEEK formulation, so direct comparisons to injection molding properties cannot be made. However, when compared to Ketaspire-810 from Solvay, the properties are comparable. They are still lower than their non-printed counterparts, but not excessively so.

Arif, et al. further showed that the raster angle has an impact on the mechanical properties of printed PEEK, corroborating Rahman, et al.'s findings [117]. Arif, et al. demonstrated that a raster angle of 0°, angled in the direction being tested, the printed part obtained 85 % of the tensile and flexural strengths of a compression molded part. These properties decreased on parts printed with a 90° raster angle, or a raster perpendicular to the testing direction. This group suggests the properties are greatly influenced by the thermal gradients across the roads of the print, and this gradient will be influenced by the build direction. The effect of print parameters like print temperature, print speed, raster angle, and layer thickness on the tensile properties of printed PEEK parts was investigated using response surface methodology (RSM) analysis [123]. The authors found that annealing the printed parts increased the crystalline content in the printed parts, thereby leading to enhanced tensile properties [123]. Liao, et al. performed similar optimization of printing parameters for MatEx of PEEK based on the Taguchi method while demonstrating the capability of printing a full-size commercial implant [161]. Moreover, they monitored the thermal history during MatEx and explored a powder spray processing step to improve biocompatibility of the printed part [161]. Optimizing print

conditions to improve tensile, bending, and flexural properties of MatEx processed PEEK has also been studied recently [162]. Annealing the printed parts can improve the mechanical performance by enhancing the interlayer coalescence but is unable to reduce the inherent porosity formed during MatEx [163]. Therefore, investigating the molecular level implications of annealing on the printed part properties is a topic of future research.

PEEK reinforced with continuous CF is an attractive choice for various industrial applications however, AM of such composites has not achieved the full potential. Currently, chopped CFs are available for PBF applications but have inferior mechanical properties due to fiber rupture and random fiber orientations during processing [164]. MatEx provides a route to print with continuous CF but early efforts have met with limited success and there is a significant difference between neat PEEK parts and their CF reinforced counterparts. Very recently, other carbon based nanomaterials like graphene nanoplatelets (GNPs) and CNTs have been used to reinforce PEEK [122]. The printed composite material had improved mechanical and tribological performance and therefore can be employed for multifunctional applications in the automotive and aerospace industries [122]. Robotic MatEx of PEEK for manufacturing thermally stable products for automated fiber placement applications is garnering attention due to the reduced coefficient of thermal expansion of the samples [121]. Although, companies like Arevo Labs and Markforged are making rapid progress in printing such materials using multi-axis robotic arms, the costs associated limits large-scale manufacturing [164].

5.4. Poly phenylene sulfide (PPS)

5.4.1. PBF

Poly (phenylene sulfide) (PPS) is the only non-PAEK high-temperature polymer reported as PBF-printable. Unlike the EOS HP3 powder, PPS printing via PBF has been published by two different research groups without using a high-temperature machine [34,92]. The paper by Ito and coauthors [92] focuses on the advantages of using a “top hat” laser beam profile, instead of a Gaussian energy profile, for printing high-temperature polymers at lower bed temperatures. Ito et al. present that the more consistent energy distribution over the laser beam diameter results in less severe energy concentrations. This allows for more energy to be delivered to the polymer optically instead of thermally. They report printing high-density parts with ultimate tensile strength of 64.5 MPa using a bed temperature of only 200 °C, i.e., 85 °C below peak melting temperature [92].

The paper by Chatham and coauthors [34] presents the process parameter selection considerations needed for processing PPS. They discuss PPS in context of both Vasquez, et al.'s SSR and Berretta, et al.'s first derivative method. The authors choose a bed temperature lower than suggested by either prediction method and report fabrication of parts with ultimate tensile strength of 61.8 MPa. This emphasizes the incomplete nature of the current process parameter value prediction literature as it fails to consider either optical or rheological properties. In addition, the authors rationalize the selection of a lower-than-theoretically-recommended bed temperature in order to extend the usable life of PPS powder. As the PBF process holds the polymer powder above T_g for a period on the order of 8–50 h, there is an increased chance of *in situ* chemical reactions and particle sintering rendering the un-fused “cake” powder no longer suitable, or at least out of specification, for printing. The wasted powder represents a significant cost and inefficiency that is more severe in high-temperature polymers than is observed in engineering-grade polymers like nylon.

Both the Chatham, et al. and Ito, et al. manuscripts read more similar to the early PEEK printing papers instead of the more current published research on printing PAEK family polymers with bed temperatures above 300 °C. It is likely the frequency of research publications centered on PBF of PPS will soon increase as Toray plastics is beginning to commercially sell a “PBF grade” PPS powder [80].

5.4.2. MatEx

Processing PPS in MatEx is challenging due to its highly semi-crystalline nature (compared with other high temperature engineering thermoplastics) and further concern with thermal crosslinking. Most of the published research on MatEx based processing of PPS have looked into optimizing the print conditions to minimize part warpage. The warpage issue of neat PPS was mathematically modeled to study the effects of thermal conductivity and coefficient of thermal expansion [165]. The simulations of the PPS parts printed using MatEx suggested that increased extrusion temperature and low deposition rate resulted in pronounced thermal variations across the part which resulted in warpage. The effect of material properties like Young's modulus and heat capacity on the printed part warpage was found to be negligible. The same group then looked at investigating the interlayer bonding in PPS printed parts using MatEx by performing a comprehensive statistical analysis [131]. They optimized the extrusion temperature as well as the post-printing heat treatment time and temperature with respect to tensile properties and percent crystallinity of the printed parts. These parameters significantly affected the interlayer bonding in the printed parts by controlling the crystallization kinetics of PPS during printing. The post-printing heat treatment increased the final crystallinity and hence improved the interlayer bonding in the printed parts. Statistical results revealed that although an extrusion temperature of 300 °C and post-printing heat treatment temperature of 180 °C was ideal for the mechanical properties. The optimum heat treatment time varied from 10 min (for tensile modulus) to 24 h (for tensile strength) depending on property under consideration.

The warpage issue can be addressed by reinforcing the PPS matrix with proper filler materials [166]. For example, in a recently reported work, 60 % by weight CF filled PPS was successfully 3D printed using BAAM for in-autoclave tooling applications at the Oak Ridge National Laboratory [132]. The fibers are responsible for distributing the redistributing residual stresses, increasing the in-plane modulus, and potentially improving the heat transfer across the polymer matrix. Kishore et al. evaluated the printability PPS and CF filled composites (30–50 wt %) [138]. The authors determined the processing window which enables the printing of these composite materials. Hassen et al. demonstrated the feasibility of using CF reinforced PPS with the BAAM process for printing large scale composite layup molds [132]. The authors found that the fibers improved heat transport during printing and the mechanical properties improved up to 50 wt% loading; however, at 60 wt% CF de-wetted, creating voids and thus a reduction in mechanical properties was observed. Another important finding was that the transient thermal variations between a new deposited road and the previous one achieved steady-state after 8–12 layers in the parts tested.

By examining a thermally activated semi-crosslinking PPS system, Geng, et al. identified the effect of post printing heat treatment on the high temperature, semi-crystalline material [133]. This group demonstrated that by reducing the amount of crystallinity during a print by using air forced cooling to increase the heat transfer coefficient, the geometric accuracy of a print could be increased. However, these samples, while geometrically accurate, possessed low tensile properties due to low crystallinity, and possibly, due to a lack of interlayer adhesion. The adhesion issue could have been caused due to limited diffusion of polymer chains since air forced cooling significantly reduced the time the polymer chains remained above T_g . By exposing the forced-air-cooled samples to an elevated temperature for 100 min, Geng, et al. was able to increase the tensile properties significantly. Heat treating at 240 °C in air for 100 min raised the crystallinity from 19.1% to 64.1% and increased the tensile strength and elastic modulus almost two-fold. A similar trend was observed in the fracture toughness, a measure of the interlayer bonding. Increasing the heat treatment temperature raised the width of the interlayer bond from 134.1–248.5 μm . The group suggests that forced air cooling to prevent or at least slow crystallization during printing, followed by a high-temperature heat treatment post-production to develop crystalline domains needed for strength and

chemical resistance properties, could be a method for printing high-temperature, semi-crystalline materials.

Ansari et al. investigated reinforcing PPS with thermotropic liquid crystalline polymers (TLCPs) by fabricating composite filaments for MatEx using the dual extrusion technology [135]. They found printing at 300 °C gave the highest properties as at higher temperatures the TLCPs undergo orientation relaxation and fiber breakage which results in inferior mechanical properties. Also the printer was able to make sharp 180° turns during MatEx and could print samples even at high loadings (67 wt%) since most of the fibers aligned along the filament length. This approach was able to print smooth parts without requiring any major printer modification and did not encounter issues like nozzle clogging and abrasion.

5.5. Polyether imide (PEI)

5.5.1. PBF

One of the most recognized members of the PEI family goes by the trade name Ultem®. Ultem is an amorphous PEI; therefore, unlike many of the other polymers discussed in this review, Ultem does not base its high-temperature properties on highly thermally stable crystal structures, but instead solely relies on its rigid molecular structure resulting from a fully aromatic backbone (shown in Fig. 2). The amorphous nature of Ultem creates significant challenges in PBF printing, as discussed in Section 3.

To the authors' knowledge, there are no published attempts at PBF printing Ultem and only one published article investigating semi-crystalline PEI for PBF printing [93]. Vaganov and coauthors processed single-layer films using the Coherent StarShape multipurpose laser machine (CO_2 laser; 10.6 μm principal wavelength) [167]. Although lacking the ability to recoat, the researchers discuss the inherent thermal and rheological properties of two PEI powders synthesized using different imidization techniques and made tensile test coupons from single-layer scans of these two powders [93]. One important concept discussed in their report is the role of crystallization kinetics on warping. The studied PEIs exhibited 51–60 % crystallinity in the powder form, but no crystalline domains were observed to form in DSC experiments cooled at 10 °C/min. Due to the short time-scale of one layer in PBF, this implies that the studied PEIs would not crystallize during the formation of a single layer. Cited literature indicates that PEIs require annealing above 280 °C for over an hour to crystallize [168]. Vaganov and coauthors report the slow crystallization kinetics as beneficial to reducing warping of polymers in PBF; in fact, it is likely the reason they were able to produce any sort of part since the StarShape machine used is not heated and fabrication was performed at room temperature [93].

Vaganov and coauthors' printed PEIs display the combination of high crystallinity in powder form with a lengthy crystallization kinetics after melting. This is, perhaps, the ideal pairing of polymer properties for PBF. Slow crystallization kinetics reduces residual stress build-up, thereby reducing warping during the coalescence and cooling step of PBF. This behavior is easily achieved with amorphous polymers; however, it is achieved at the expense of the crystallinity needed for selectivity during energy input via laser scanning. Vaganov and coauthors' PEIs exhibit the rare combination of these inherent polymer properties promoting printability.

5.5.2. MatEx

MatEx based printing of Ultem has been quite successful as material warpage resulting from crystallization from the melt does not interfere with the process. Ultem 9085 was successfully printed using a Fortus 400 mc MatEx printer to investigate its dynamic loading properties [126]. The printed parts had significant surface roughness which affected the tensile properties. The authors suggested the use of chemical smoothing of the parts that resulted in increase of tensile strength and ultimate strain by 16 % and 24 % respectively in the + z-axis build

direction. The improvement in properties were probably due to a decrease in external notches after treatment which smoothed the print surface.

The effect of processing and different print orientations on the mechanical properties of Ultem 9085 was studied in greater detail by Zaldivar et al. [127]. They used the print settings similar to those used by Fischer & Schöppner [126]. A key finding from their results was that the parts printed with an orientation that permitted the layup of extruded fibers along the load direction showed better mechanical performance than those printed with fibers in the orthogonal-to-load direction. Depending upon the print direction the parts could achieve 46–85 % of the properties obtained by injection molding Ultem 9085. Similar work with Ultem 9085 filaments investigated the effect of layer orientation and build direction on the mechanical properties of the printed parts using a Stratasys Fortus 450mc printer [128]. The researchers found that the 0°-layer orientation and edge build direction resulted in parts with maximum tensile strength. They attribute this to increased layers along the width of the parts and tightly packed structure in the direction of tensile testing. The effect of different solvent treatments on the mechanical properties of 3D printed Ultem 9085 parts was investigated by de Bruijn et al. [169]. The goal of the study was to identify a solvent that can successfully dissolve support materials without significantly affecting the printed part properties (tensile and flexural). A recent study examined the development and characterization of composite PEI (Ultem 1010) filaments for MatEx based AM for applications in thermal protection systems [170]. Although the researchers were able to get accurate filament dimensions required for MatEx, they did not look into the mechanical properties of the parts manufactured using the technique.

Additively manufactured Ultem 1010 is another promising material for high temperature applications but limited knowledge about the creep behavior and availability have restricted its widespread use [73]. However, there are some literature available for MatEx of Ultem 1010. Taylor et al. investigated the flexural properties of Ultem 1010 parts through a full factorial design of experiments (DOE) and optimized the print parameters [171]. The experimental findings were corroborated with three dimensional non-linear thermomechanical finite element modeling [171]. Further, the fracture toughness of MatEx processed Ultem 1010 parts has been optimized with respect to build orientation and raster angle by employing a similar DOE approach [172]. Defects in intra- & interlayer bonding as well as individual raster were the main causes of failure of the printed samples. Han et al. designed a laser system for Ultem 1010 that heated up the extrudate prior to deposition on the printer bed [173]. The laser assisted heating resulted in an increase in interlayer bonding, which was attributed to improved healing at the interface. The effect of print temperature and print orientation on the material properties of Ultem 1010 has also been investigated and parts with ~80 % of the injection molded properties were obtained [162].

Carbon nanofiber filled composites of Ultem 1000 has been printed using a custom built MatEx printer capable of handling heat resistant thermoplastics [125]. The researchers looked into the effect of CF loading on the mechanical properties of the nanocomposite and they found that at 1 wt% loading the properties of the MatEx printed composite parts were similar to those obtained using injection molding. The properties of the composites were higher than that for pure Ultem 1000 due to the reinforcement provided by the nanofiber orientation along the filament [125]. Ultem 9085 and Ultem 1000 along with their composites with chopped CFs have been studied in MatEx to produce components for aerospace applications [124]. MatEx printing resulted in a significant reduction (~50–67%) in the length of the CFs (known as fiber attrition) present in the composites. Therefore, it is important to achieve an optimum fiber loading that can assist the stress distribution and improve the heat transfer while retaining their intrinsic dimensions. Addition of CFs was also found to lower the tensile strength of the filled Ultem 1000 composites which the authors attribute to the

formation of a porous matrix in the composite due to entrapped moisture within the filament and degradation occurring inside the liquefier of the printer [124]. The higher melt viscosity of Ultem 1000 composites meant that it had to be printed at 420°C rather than at 375°C which was used for Ultem 9085. The higher processing temperature led to an enhanced volumetric expansion of the water trapped within the filament thereby increasing the porosity of the system further. Therefore, the polymer flow characteristics can also significantly affect the part properties after print. Recent work has investigated CNT reinforced Ultem 1000 composite filaments as a potential material for MatEx [174]. The composites had uniformly dispersed and aligned CNTs in the PEI matrix which improved their tensile strength; however, during melt compounding the length of the CNTs reduced due to exposure to high shear stresses [174].

Because the temperatures at which PEI are generally processed and conventionally manufactured are different from that required in MatEx, it is important to study the effect of the MatEx parameters on the part strength of PEI and understand how the properties change when it is subjected to such processing conditions. Wu et al. looked into the effect of printing temperature on the strength of the interlayer bonding in 3D printed thermoplastic polyimide parts [175]. They found that with increasing the printing temperature from 320°C to 335°C resulted in an improvement in interlayer bond performance due to increased interlayer bonding area since the cooling rate was lower at higher temperatures and thus more time was needed for the bonds to consolidate. Printing at temperatures higher than 340°C resulted in poor quality prints due to poor interfacial bond strength as the viscosity increased drastically, possibly due to crosslinking reactions, that eventually lead to materials foaming. The process parameters needed to produce parts for widespread applications in the industrial sectors was obtained from this study.

Ajinjeru et al. established the proper processing conditions in MatEx for PEI (Ultem 1000) using thermal characterizations techniques [176]. Rheological results on PEI and short carbon-fiber reinforced PEI composites at different temperatures and shear rates revealed that the processing conditions had a profound impact on the flow behavior of the polymer melt and a comprehensive understanding is required to further optimize the printing process. Increase in CF loading in the PEI matrix resulted in an expected increase in complex viscosity. The authors anticipated the actual viscosity of the composites during the printing process at steady state to be lower than the reported values due to the alignment of the CFs in the direction of shear. The results from this study showed that an extrusion temperature of 400°C, where the complex viscosity reduced by ~50 %, can be used BAAM of CF reinforced PEI under a shear rate of ~100s⁻¹. Also, the flow behavior and viscosity of CF reinforced ABS was found to be in the vicinity of PEI and it was postulated that both the materials can be printed successfully using BAAM, although there remained scope for further work on this topic.

Recent work has focused on fabrication of PEI filaments for MatEx by blending it with polycarbonate (PC) to produce an immiscible blend [177]. The incorporation of PC in the PEI matrix lowers the viscosity of the blend which makes it easier to process in the extruder. However, the researchers only explored the potential of such blends in MatEx by analyzing the thermal properties and did not actually print with them [177]. They also recommended to investigate PEI/PC blends in presence of a suitable compatibilizer to further assist processing.

Based on the promised usefulness of MatEx printing with PEI, the government institute America Makes led a program towards understanding the behavior of Ultem 9085 when printing using a Stratasys Fortus 900mc [178]. Knowledge gained from the project will aid in the understanding of part-to-part variation, build-to-build variation, and printer-to-printer variation. Each of these components are key to certifying additively manufactured Ultem, thereby expanding the potential of high-temperature polymers in AM.

6. Machine capabilities

Modifications to standard machine design are made for both PBF and MatEx printing technologies in order to accommodate the additional challenges of printing high-temperature polymers. As previously discussed in Section 4, some of the properties perceived as benefits for end-use applications add to the challenge of processing. This section provides an overview of published research regarding printer-centric solutions or processing techniques to manage the high-performance properties of high-temperature polymers during printing.

6.1. Machine capabilities in PBF

While each of the three sub-functions are present in all technologies classified as PBF, only the original Polymer Laser Sintering technology includes a heated build chamber. It is therefore unsurprising that no high-temperature polymers have been reported as printed using either High-Speed Sintering or Multi-jet Fusion. Published literature emphasizes the importance of the chamber temperature is not only for melting, but for minimization of thermally induced stress [179]. If the stress is too great, it will cause the part to warp out of plane, potentially leading to part failure. Therefore, there is still an emphasis in printing high-temperature polymers at bed temperatures near the melting temperature of the polymer, i.e., 285–350 °C for PPS, PEEK, and PEK. A few notable exceptions are Niino and coauthors who have shared results concerning printing PEEK [86] and PPS [92] at 200 °C, and Chatham, et al. reporting printing PPS at 230 °C [34].

Although much of the more recent high-temperature polymer printing has focused on using the EOS P800 with its high-temperature build chamber, it is worth noting the earlier successes with printing high-temperature polymers at lower temperatures on what might be considered a standard machine. These researchers report compensating for their inability to heat the polymer with the build chamber by increasing the optical energy supplied via laser scanning. Based on the optical energy density equation (Eq. 9), one observes the positive relationship between laser power and total energy density and the inverse relationship between scan speed and energy density [180].

$$E_D = \frac{P_L}{d_L \times h_s \times v_s} \quad (9)$$

where E_D is energy density, P_L is laser power, d_L is diameter of the laser beam, h_s is hatch spacing, and v_s is beam speed. A slower beam speed results in more total energy and is therefore a potential alternative avenue to investigate for printing high-temperature thermoplastic polymers. Decreasing the hatch spacing so that the beam diameter makes multiple passes over the same area and increasing laser power are other ways to increase the total optical energy delivered by the machine during fabrication. However, this is dependent on the thermal conductivity, CTE, and crystallization kinetics of the polymer as re-coating comparatively cold powder overtop of a freshly scanned laser may introduce severe thermal gradients leading to residual stress and out-of-plane warping. Further research is needed to determine if this processing technique can be generalized for all high-temperature polymers.

Ghita and coauthors report that the EOS P800 was the only commercially available PBF machine capable of printing high-temperature polymers, as it is the only machine able to reach temperatures in excess of 350 °C [87]. One custom built machine was made by placing an additional heater in the central build area of an existing EOSINT 380 [156]. The modifications allowed the build chamber to reach 250 °C. These researchers successfully used their modified commercial machine to print PEEK despite this being nearly 100 °C cooler than using an EOS P800.

Fish and coauthors describe their process of designing and constructing a machine to print PEEK and PAEK [181]. The laser AM pilot system (LAMPS) team increased the processing temperature

approximately 200 °C from the “standard” machines for polyamide printing. The LAMPS has higher power heating elements and additional insulation to enable the build surface temperature to approach the melting temperature of PEEK. In their publication, Fish et al. comment that radiation-based heating of the build surface leads to poor temperature consistency across the build volume as it unduly emphasizes the temperature at a specific area. The LAMPS team designed the machine to inhibit convection inside the build chamber to promote consistent temperature across the chamber [181].

A second priority for the LAMPS team was to minimize feed temperature exposure for powder longevity [181]. A challenge with all thermoplastic polymers is molecular weight stability over time. The polymer's molecular weight tends to become less stable the longer it is held at temperatures above its T_g . Therefore, powder reuse can be a more prominent concern when printing high-temperature polymers than when using the standard polyamide. In addition, high-temperature polymer powders are often significantly more expensive, therefore a long lifespan of continued reuse would be of great benefit. The LAMPS design team isolates the feed powder from the build area through a drop feeding system instead of piston feed. They claim that a drop feeder is easier to insulate and helps to rapidly heat powder through natural convection as the polymer powder drops into place. The drop height was designed so that the new powder layer is very nearly the same temperature as the powder in the build area. This is important, else the presence of relatively colder powder can result in warp and failure inducing thermal gradient [179].

One of the expenses in building a high-temperature PBF machine is the importance of maintaining an inert atmosphere inside the printer. The rubber gaskets and seals that create a gas-tight chamber must be rated for use at the extreme processing temperatures. The inert environment is critical for polymers to avoid thermo-oxidative degradation during the manufacturing process [181].

6.2. Machine capabilities in MatEx

The first description of a MatEx AM system having the capability to handle thermoplastic materials that need to be processed at high temperatures was reported in a 2004 patent disclosure [182]. The inventors described printing inside a chamber heated above the solidification temperature of the material that is being printed to address the issues arising from stress build-up and thereby reduce the part warpage and distortion. By controlling the build environment temperature, parts can be printed from materials that stress relax at relatively high temperatures. Precautions such as insulating the motion controllers that helped to dispense material on the printer bed were taken so that the high environmental temperature cannot have a detrimental effect on the service life of the controllers. Further work on the details of the printing method using high temperature materials was done by the same group [183].

With the rapid development of MatEx printers for high temperature materials, several manufacturers currently advertise machines that have the desired capability. Table 5 lists some of the MatEx based commercially available printers along with their build volume, compatible high temperature thermoplastic materials as well as specifications like the maximum temperature of extruder, print bed and build chamber. Most of these printers have been designed to print high temperature thermoplastic materials like PEEK, PEI, and CF reinforced composites of the same material. The heated chamber in the printers helps to ensure adequate adhesion between the printer bed and the first layer of material deposited as well as enhanced interlayer adhesion which minimizes part deformation and delamination during the course of the printing process.

Other than using commercial MatEx machines, academic research has led to the designing of different custom-built printers that are suitable for high temperature thermoplastics as well. Vaezi and Young [116] had designed two different MatEx based systems (syringe and

Table 5

Commercially available MatEx printers suited for high temperature materials.

Printer	Build volume (mm)	Max. extruder temperature (°C)	Compatible materials	Max. print bed temperature (°C)	Max. build chamber temperature (°C)	Country
AON 3D AON-M2	457 × 457 × 635	470	PEEK, PEI, PPS, PPSU	200	120	Canada
Apium P220	145 × 135 × 148	520	PEI, PEEK, PEEK + CF	160	180	Germany
Cincinnati SAAM HT	200 × 190 × 240	500	PEEK, PEI, PEEK + CF	250	110	USA
Dynamical Tools HT 45	450 × 300 × 300	500	PEEK	200	200	Spain
Hyrel 3D System 30	225 × 200 × 200	450	PPS	80	55	USA
IEMAI Magic HT Pro	310 × 310 × 480	450	PEEK, PEI	170	120	China
INTAMSYS FUNMAT HT	260 × 260 × 260	450	PEEK, PEI, PPSU	160	90	China
miniFactory Ultra	330 × 180 × 180	470	PEEK, PEKK, PEI	250	250	Finland
Oo-kuma KATANA	200 × 200 × 185	480	PEI, PEEK, PEEK + CF	120		Turkey
Qualup Qu3 HT	300 × 250 × 300	500	PEKK, PEEK, Ultem	275	275	France
Roboze One + 400	300 × 300 × 200	500	PEEK	130		Italy
Rokit 3Dison AEP	230 × 200 × 200	400	PEI	160		Korea
Stratasys Fortus 400mc	914 × 600 × 914	225	PEI, PPSU		225	USA
Tractus3D T650P	170 × 170 × 285	450	PEEK, PEI	175	65	Netherlands
VeraShape VSHAPER Pro	260 × 260 × 185	430	PEEK	150		Poland

filament based) capable of printing PEEK. They modified an UP 3D printer such that the extrusion and printer bed temperature reached 460°C and 130°C respectively. An ambient temperature of 80°C was maintained to help with the relieve stress build-up using heating lamps. Yang et al. [109] independently developed a novel temperature controlled MatEx system that was used to print PEEK. This system had greater operational flexibility as the extrusion temperature could be varied from 360°C to 500°C and the ambient temperature from 25°C to 200°C depending on the material. In addition, the machine had the capability of performing post-printing heat treatments which had a favorable effect on the mechanical properties of the PEEK printed parts.

PEEK (Victrex 450 PF grade) filaments were printed by MatEx using a nozzle diameter of 0.4 mm with an optimized print speed of 20 mm/s; nozzle temperature of 400°C and printer bed temperature of 100°C [110]. A novel screw extrusion system capable of printing at 380°C was designed to print PEEK using pellets instead of filaments thereby eliminating a pre-processing step in MatEx [184]. The basic principle of this system was similar to the syringe-based system reported by Vaezi and Young [116]. In a recent study by Arif et al., PEEK was printed by MatEx using a benchtop Indmatec HPP 155 device with extruder nozzle of 0.4 mm; a print temperature of 410°C and build plate temperature of 100°C [117].

MatEx based printing using carbon nanotube filled PEEK had also been investigated using a MendleMax v2.0 printer from Maker's Tool Works [118,119]. As the machine had a simple operating procedure, the authors modified the extrusion head with an E3D online V6 all metal hot-end. Also, the print bed was custom built with aluminum to get to higher temperatures (300°C) than what the commercial machine offers. Processing PEEK was further facilitated since this system had stainless steel tubing rather than the commonly used PTFE lining that is prone to abrasion. Printing with PEEK/CF composites has also been reported with a custom-made FDM Z2 3D printer which has an extrusion temperature of 380°C and a bed temperature of 95°C [185]. The nozzle of the printer was modified appropriately to include a proper K-type thermocouple which could withstand the high processing temperatures of PEEK. A recent study investigated the effect of extrusion speed, nozzle diameter, extrusion multiplier, and printing speed on the filament dimensions after extrusion through the nozzle using an in-house printer having a nozzle temperature of 360°C [186]. The build volume of this printer (300 × 300 × 200 mm³) is comparable to some of the commercially available high temperature 3D printers listed in Table 5.

Zawaski and Williams recently developed a novel inverted MatEx system to print engineering thermoplastics at significantly lower costs than the commercially available MatEx printers [187]. The advantage of the inverted system is two-fold; firstly, it protects the electrical components from getting damaged at high print temperatures and secondly, it helps to entrap heat in the build chamber thereby minimizing thermal fluctuations. The system was able to maintain build temperatures around 400°C and the authors demonstrated the applicability of this design by printing both tensile bars and complex geometries polyphenylsulfone (PPSF).

Another high-performance thermoplastic polymer PPS has been successfully printed by MatEx using HYREL System 30 from the company HYREL 3D [131]. The printer can handle a maximum extrusion temperature of 450°C and the build plate as well as the chamber temperature can be modified during the printing process. PPS and PEKK as well as their composites with CF were printed with a customized Solidoodle 3 printer modified with a E3D V6 all metal hot-end [138]. The printing temperature for pure PPS and PEKK was in the range of 280–290°C and 390–400°C respectively.

Thermoplastic polyimide has also been printed by MatEx using a custom-built 3D printer with a print temperature of 320–340°C; but since it is an amorphous polymer that does not suffer from the warpage issues the print chamber temperature was kept at 25°C [175]. A modified Lulzbot Taz 4 3D printer with a high temperature hot end has been used to print high quality warp free parts from Ultem 1010 [188]. The extrusion nozzle temperature was in the range of 345–375°C while the bed temperature was varied from 155–200°C. Infrared heating lamps were also installed inside the printing chamber in order to have better control over the part temperature during the print. Using a similar Lulzbot Taz 6 system equipped with environmental heating Gilmer et al. [189] printed single road width walls from Ultem 1010 filaments at 350°C with a bed temperature of 200°C.

7. Challenges in printing with high temperature engineering thermoplastics

7.1. PBF challenges

The challenges facing the field of high-temperature polymer PBF can be grouped into machine-related and polymer-related challenges; although, these are linked. The machine challenges are, for the most part, shared by all high-temperature polymer processing. These

challenges include the need to heat certain areas of the machine while insulating critical areas, such as electronics housing and the operator's viewport. In PBF, there is also the need to insulate, or at least maintain a cooler temperature, of the feed powder until it is time for spreading across onto the build piston. This is perhaps more challenging than molding processes where the timescale of the process is shorter, as is the case for injection molding, or else all the charged polymer powder is used, as is the case with rotational molding. In PBF, the desire to reclaim and reuse the unfused powder in future builds is reportedly more difficult with most these high-temperature polymers than with polymers like nylon-12. The key properties for successful PBF manufacturing are dependent on the time a polymer is held above its T_g . Additional studies concerning powder lifespan are needed for each chemically unique polymer. The work leading to the commercialized PEKK co-polymer affects powder lifespan by reducing T_m and therefore the required processing temperature [37]. However, similar effects may be realized through including photo-absorbing additives [190] or viscosity modifiers to more efficiently and selectively coalesce particles without altering the chemical structure of particles in the feed or surrounding cake. This may also be achieved through innovative ideas on how to mechanically insulate feed powder during processing and design more chemically robust polymers for the long timescale of PBF processing are needed.

Another machine-related topic for future work is understanding when to use the heaters and when to use the laser beam to supply the energy needed to melt and fuse the polymer powder. This topic for future investigation is not specific to high-temperature thermoplastics, but it has potentially greater significance for their processing. The ability to supply a greater percentage of energy optically instead of thermally will aid in prolonging the lifespan of unfused powder by keeping the powder at a lower temperature throughout the build. This is due to the inherent greater selectivity of energy delivery of a laser beam as compared to heaters. Relying on the laser beam to a greater extent also enables PBF printing of high-temperature polymers on less expensive machines that were originally developed to print polyamides. A statistical design of experiments focusing on delivering the same amount of total energy through different combinations of optical and thermal component energy for each high-temperature polymer would reveal the interplay between each energy type and evaluate feasibility of relying on optical energy in manufacturing.

Conversely, further exploration may confirm that high build chamber temperatures are required for geometrically accurate production and reduced warping arising from differential thermal stresses between the heated melt-pool and relatively cooler surrounding powder. The HSS and MJF technologies increase heater selectivity by jetting photothermal ink into the powder bed. Future research is needed to determine if these inks may be effective at locally raising temperature to enable complete coalescence. The inherent trade-off for these technologies is loss of purity in your final part.

The authors purport that the primary material related challenges to printing high-temperature polymers via PBF are (i) powder manufacture and (ii) consistency in published reporting. Producing powdered polymers is also a challenge for industries like rotational molding and powder coating. However, the primary property in those industries is size. PBF adds the complexity of solid-state powder flow during the recoating sub-function. This imposes not only size requirements, but also requirements preferring spherically shaped powders. One advantage high-temperature polymers have over materials like polyamides is their high T_g makes it easier to produce powders through grinding. The work of Berretta and coauthors is leading the field in this topic [191]. They explored the commercial PBF grade PEK powder, HP3, as well as two commercial grades of PEEK, Victrex 150 PF and 450 PF, that were not marketed as "PBF-grade." They report that non-PBF grades were not optimized for flowability in the machine, but were optimistic of future refinement enabling high quality printing.

Finally, an awareness of the PBF materials development literature is

critical for this field to continue to advance. As people are aware of the work of Vasquez, et al. in their energy melt ratio [32] and consistently report all relevant process parameter values, the opportunities for synthesis of guidelines for structure-property-process-property relationships will increase. These are the pieces of fundamental polymer manufacturing science that will drive the expansion of the PBF material catalog. In turn, the increased variety of materials will provide additional opportunities for expanded industrial applications as the material selection process approaches that of mainstream manufacturing methods, like injection molding.

7.2. MatEx challenges

The commercially available high temperature polymers for processing in MatEx are all modified to a certain extent. For example, many of the Ultem grades are a blend of PEI and PC while filaments of PEEK invariably contain different additives that impact the crystallization mechanism. Unfortunately, these compositions are only known to the manufacturers and hence the print conditions that work for these materials often fail for neat polymers.

Moreover, printing high temperature engineering thermoplastics using MatEx require printers that are equipped to handle them. These printers do exist (e.g. HYREL, Stratasys) as listed in Table 5 but their use has been limited due to complications associated with machine certification, print precision, repeatability, and build size. For example, the optimal environmental temperature as reported in a recent study for printing PEEK [109] can only be reached by those printers in Table 5 with high-temperature environment chamber. However, it is still difficult to consistently maintain high temperature ($> 250^\circ\text{C}$) during printing of the high temperature engineering thermoplastics. The machine limitation can only be addressed by designing better configurations that allow for easy monitoring and control of parameters during the MatEx process. Currently, MatEx technology has limited capability to monitor and control the temperature profile inside the nozzle during the print, although significant progress has been made recently to track changes in pressure and temperature by innovative nozzle designs and better thermal characterization techniques [192–195]. The cost of incorporating the additional functionalities required for high temperature polymers into a printer is a significant limitation [196]. Finally, some of the high temperature printer designs have been patented and have intellectual property restrictions which has prevented their widespread use. Therefore, the main challenges faced by the researchers are access to machines that are compatible with the high processing temperatures of the materials.

The reduction in mechanical properties of MatEx processed parts is particularly unacceptable when producing parts from high temperature engineering thermoplastics that require to have excellent mechanical properties under high thermal loads. The larger thermal gradients and corresponding CTE mismatch aggravates the problems for high temperature thermoplastics compared to polymers that are processed at lower temperatures when printing parts of any significant size. Fitzharris' work with PPS shows the CTE is that material property that results in the largest impact on part warpage and thus residual stresses [165]. Increasing the print speed or layer height can decrease the warpage by decreasing the thermal gradient within a layer [197] and increasing the environment temperature increases the bonding [198]. Finally, the part geometry also influences the time between layers. Longer time between layers causes the layers to cool and significant pauses between layers can cause the part to fail sooner [199].

The thermal profile during printing is of importance as it controls the residual stress build-up and interlayer bonding in the part. Since most of the high temperature engineering polymers discussed in this review are semi-crystalline which exhibit a high degree of crystallinity and high shrinkage coefficient, processing these materials using the MatEx technique is challenging as the contraction in volume during the print can have an adverse effect on the geometric and dimensional

accuracy of the printed parts [200]. Researchers have been successful in addressing these problems by printing on a heated printer bed and modifying the environmental conditions inside the printer chamber [43,201].

Fillers are often incorporated to counter some of the CTE mismatch in MatEx for high temperature engineering thermoplastics. They improve the mechanical performance of materials as well as reduce shrinkage and warpage by either controlling the crystallization kinetics or by relieving trapped residual stresses. Recently efforts have been directed at fabricating nanocomposite filaments, where the fillers are generally carbon-based materials like carbon fiber [202] graphene [203,204] or CNT [205], for application in MatEx due to their excellent mechanical, thermal and electrical properties. Love et al. demonstrated how the addition of CFs can greatly reduce warping of printed parts by increasing the thermal conductivity and reduced CTE [206]. The change in these parameters aids in minimizing the thermal gradients within printed parts, thus reducing uneven shrinkage/warpage. Love's findings, although not directly performed on high-performance thermoplastics, this work shows the importance of providing solutions for printing high performance thermoplastic materials which have unfavorable CTE and thermal conductivities.

8. Conclusions

In the current review article, the current state of the art for high-temperature (i.e., traditional processing temperature $> 250^{\circ}\text{C}$), thermoplastic polymers in the MatEx and PBF modes of AM have been assessed. Commercially available printers utilizing both the MatEx and PBF technologies can process high-temperature engineering polymers, along with specialized versions that have been modified to serve specific research purposes. Thermoplastic processing generally follows a heat-and-reform paradigm to overcome the high viscosity of high-temperature polymers; therefore, most alterations to machine designs involve insulated chambers that efficiently heat the polymer to remove barriers to flow (e.g., crystalline regions and high viscosity) and minimize thermal gradients that induce residual stress inside the part as it is formed. This must be achieved while simultaneously protecting the sensitive electronics that enable precise manufacturing. Control over the temperature distribution during the print is important to achieve the best possible mechanical properties and maintain dimensional accuracy.

Although physics-based understanding and implementation of both PBF and MatEx are emerging, most studies continue to look at the effect of print parameters on printed part properties and evaluate "printability" by trial and error. The currently identified key properties for both AM techniques, as well as the impact of structure features common to high-temperature polymers on these "printability" related properties, are discussed in this paper. Due to AM's layer-wise paradigm, key polymer properties for suitable AM feedstock will include properties traditionally associated with bulk processing (e.g., melt viscosity at a given shear rate) and properties traditionally associated with adhesion science (e.g., surface energy). In addition, the elements of discrete and layer-wise heating render many steady-state approximations of polymer properties less useful. We know from adhesion mechanics that differences in properties like stiffness and thermal expansion between bonded materials introduce residual stresses that may result in failure. Similar failure may occur in AM with polymers demonstrating a strong temperature dependence in these properties if the difference in temperature between adjacent layers is above a critical value. This typifies the challenge exacerbated by high temperature polymers that force large temperature gradients.

The selection of polymer families investigated in the AM literature are those of industrial relevance to the early adopter industries of defense, aerospace, automotive, and biomedical. Most research groups and related publications studying AM of high-temperature polymers focus on the poly(arylene ketone) family, including PEEK, PEKK, and

PEK. The PEI family, including Ultem, is the second most investigated polymer for MatEx due to its importance in aerospace and selection by America Makes as the test-case for round robin study on AM viability. Because PEI polymers are typically amorphous, there has been very little work published on PEI in PBF. AM of PPS has been reported in the literature for both PBF and MatEx techniques; however, it is currently the least studied of the high-temperature polymer families identified as printable.

Current research opportunities are limited by the availability of high-temperature machines and AM-grade high-temperature polymer feedstock; however, publications in this area should increase as additional polymer suppliers and machine manufacturers enter the field. For example, the authors expect to see an increase in publications of printing PPS by PBF with Toray releasing a "laser sintering grade" PPS powder for purchase and as more laboratories obtain access to machines like the EOS P800. A similar expectation exists for filled polymer systems. While pellet-fed extrusion systems, like BAAM, can use the existing composite polymers for injection molding supply chain, composite feedstocks are less readily available for filament-based extruder systems and PBF.

High temperature engineering polymer composites have the potential to meet industrial needs for part performance; however, additional understanding must first be gained on the interplay between AM process physics and polymer physics before scientific breakthroughs can be realized for more complex systems. Further research must be performed in investigating the fundamental polymer properties and modifications to develop a predictive capability that can ensure successful processing of high temperature engineering thermoplastics in AM. Advancements in the understanding of polymer behavior during AM, including *in situ* morphology development and rheological behavior, are the next step toward effective quality control programs and informing computer aided engineering (CAE) simulation software. These are the types of advancements needed to transition AM of high-temperature engineering polymers into an industrial-scale production reality.

Declaration of Competing Interest

The authors declare that they have no known competing financial interests or personal relationships that could have appeared to influence the work reported in this paper.

Acknowledgements

A.D. would like to acknowledge funding from the Adhesives and Sealants graduate research assistantship from the Macromolecules Innovation Institute (MII) at Virginia Tech. C.A.C. would like to acknowledge funding from the Department of Energy's Kansas City National Security Campus, operated by Honeywell Federal Manufacturing & Technologies, LLC under contract number DE-NA0002839. All the authors would also like to acknowledge the MII at Virginia Tech for providing the collaborative infrastructure at Virginia Tech focused across the spectrum of polymer science and engineering.

References

- [1] A. Gebhardt, Understanding Additive Manufacturing: Rapid Prototyping, Rapid Manufacturing, and Rapid Tooling, (2012), pp. 40–44.
- [2] T.J. Horn, O.L. Harrysson, Overview of current additive manufacturing technologies and selected applications, *Sci. Prog.* 95 (2012) 255–282.
- [3] V. Mironov, R.P. Visconti, V. Kasyanov, G. Forgacs, C.J. Drake, R.R. Markwald, Organ printing: tissue spheroids as building blocks, *Biomaterials* 30 (2009) 2164–2174.
- [4] Y. Huang, M.C. Leu, J. Mazumder, A. Donmez, Additive manufacturing: current state, future potential, gaps and needs, and recommendations, *J. Manuf. Sci. Eng.* 137 (2015) 014001.
- [5] J. Choi, O.-C. Kwon, W. Jo, H.J. Lee, M.-W. Moon, 4D printing technology: a review, 3D printing and additive manufacturing, *3D Print. Addit. Manuf.* 2 (2015)

159–167, <https://doi.org/10.1089/3dp.2015.0039>.

[6] B. Gao, Q. Yang, X. Zhao, G. Jin, Y. Ma, F. Xu, 4D bioprinting for biomedical applications, *Trends Biotechnol.* 34 (2016) 746–756, <https://doi.org/10.1016/j.tibtech.2016.03.004>.

[7] M. Beecroft, 3D printing of weft knitted textile based structures by selective laser sintering of nylon powder, *IOP Conf. Ser.: Mater. Sci. Eng.* 137 (2016) 012017, , <https://doi.org/10.1088/1757-899X/137/1/012017>.

[8] B.G. Compton, J.A. Lewis, 3D-printing of lightweight cellular composites, *Adv. Mater.* 26 (2014) 5930–5935, <https://doi.org/10.1002/adma.201401804>.

[9] Indaero 3D Printing Case Study, Stratasys. (n.d.). <https://www.stratasys.com/resources/search/case-studies/indaero> (Accessed September 18, 2019).

[10] A.M. Forster, Materials testing standards for additive manufacturing of polymer materials: state of the art and standards applicability, *Additive Manufacturing Materials*, (2015), pp. 67–123.

[11] D. Deng, Y. Chen, C. Zhou, Investigation on PEEK fabrication using mask-image-projection-based stereolithography, *Annual Solid Free Form Fabrication Symposium* (2012) 606–616.

[12] D. Bourell, J.P. Kruth, M. Leu, G. Levy, D. Rosen, A.M. Beese, A. Clare, Materials for additive manufacturing, *CIRP Ann.* 66 (2017) 659–681.

[13] S.C. Ligon, R. Liska, J. Stampfl, M. Gurr, R. Mülhaupt, Polymers for 3D printing and customized additive manufacturing, *Chem. Rev.* 117 (2017) 10212–10290.

[14] S. Singh, S. Ramakrishna, R. Singh, Material issues in additive manufacturing: a review, *J. Manuf. Processes* 25 (2017) 185–200, <https://doi.org/10.1016/j.jmapro.2016.11.006>.

[15] T.D. Ngo, A. Kashani, G. Imbalzano, K.T.Q. Nguyen, D. Hui, Additive manufacturing (3D printing): a review of materials, methods, applications and challenges, *Comp. Part B* 143 (2018) 172–196, <https://doi.org/10.1016/j.compositesb.2018.02.012>.

[16] R.D. Goodridge, C.J. Tuck, R.J.M. Hague, Laser sintering of polyamides and other polymers, *Progr. Mater. Sci.* 57 (2012) 229–267.

[17] C.A. Chatham, T.E. Long, C.B. Williams, A review of the process physics and material screening methods for polymer powder bed fusion additive manufacturing, *Progr. Polym. Sci.* (2019).

[18] D. Popescu, A. Zapciu, C. Amza, F. Baciu, R. Marinescu, FDM process parameters influence over the mechanical properties of polymer specimens: a review, *Polym. Test.* 69 (2018) 157–166, <https://doi.org/10.1016/j.polymertesting.2018.05.020>.

[19] H. Klippstein, A.D.D.C. Sanchez, H. Hassanin, Y. Zweiri, L. Seneviratne, Fused deposition modeling for unmanned aerial vehicles (UAVs): a review, *Adv. Eng. Mater.* 20 (2018) 1700552, , <https://doi.org/10.1002/adem.201700552>.

[20] K.S. Boparai, R. Singh, H. Singh, Development of rapid tooling using fused deposition modeling: a review, *Rapid Prototyp. J.* 22 (2016) 281–299.

[21] L.K. Prasad, H. Smyth, 3D printing technologies for drug delivery: a review, *Drug Dev. Ind. Pharm.* 42 (2016) 1019–1031, <https://doi.org/10.3109/03639045.2015.1120743>.

[22] J. ten Kate, G. Smit, P. Breedveld, 3D-printed upper limb prostheses: a review, *Disabil. Rehabil.* 12 (2017) 300–314, <https://doi.org/10.1080/17483107.2016.1253117>.

[23] A.M. Peterson, Review of acrylonitrile butadiene styrene in fused filament fabrication: a plastics engineering-focused perspective, *Addit. Manuf.* 27 (2019) 363–371, <https://doi.org/10.1016/j.addma.2019.03.030>.

[24] X. Wang, M. Jiang, Z. Zhou, J. Gou, D. Hui, 3D printing of polymer matrix composites: a review and prospective, *Comp. Part B* 110 (2017) 442–458.

[25] S. Yuan, F. Shen, C.K. Chua, K. Zhou, Polymeric composites for powder-based additive manufacturing: materials and applications, *Prog. Polym. Sci.* 91 (2019) 141–168, <https://doi.org/10.1016/j.progpolymsci.2018.11.001>.

[26] C.R. Deckard, Method and apparatus for producing parts by selective sintering, 4, 863,538, 1989.

[27] N. Hesse, M.A. Dechet, J.S.G. Bonilla, C. Lübbert, S. Roth, A. Bück, J. Schmidt, W. Peukert, Analysis of tribo-charging during powder spreading in selective laser sintering: assessment of polyamide 12 powder ageing effects on charging behavior, *Polymers* 11 (2019) 609, <https://doi.org/10.3390/polym11040609>.

[28] M. Van den Eynde, Expanding the Polymer Material Palette for Laser Sintering: the Importance of Powder Flowability, *PhD Thesis KU Leuven*, 2018.

[29] S.B. Liang, D.P. Hu, C. Zhu, A.B. Yu, Production of fine polymer powder under cryogenic conditions, *Chem. Eng. Technol.* 25 (2002) 401–405, [https://doi.org/10.1002/1521-4125\(200204\)25:4<401::AID-CEAT401>3.0.CO;2-S](https://doi.org/10.1002/1521-4125(200204)25:4<401::AID-CEAT401>3.0.CO;2-S).

[30] D. Drummer, M. Medina-Hernández, M. Drexler, K. Wudy, Polymer powder production for laser melting through immiscible blends, *Procedia Eng.* 102 (2015) 1918–1925, <https://doi.org/10.1016/j.proeng.2015.01.332>.

[31] M.A. Dechet, S. Kloos, W. Peukert, J. Schmidt, Production of spherical micron-sized polymer particles for additive manufacturing by liquid phase processes, *AIP Conference Proceedings*, (2019), <https://doi.org/10.1063/1.5084905> 140002.

[32] M. Vasquez, B. Haworth, N. Hopkinson, Optimum sintering region for laser sintered nylon-12, *Proc. Inst. Mech. Eng. Part B* 225 (2011) 2240–2248, <https://doi.org/10.1177/0954405411414494>.

[33] M. Vasquez, B. Haworth, N. Hopkinson, Methods for quantifying the stable sintering region in laser sintered polyamide-12, *Polym. Eng. Sci.* 53 (2013) 1230–1240, <https://doi.org/10.1002/pen.23386>.

[34] C.A. Chatham, T.E. Long, C.B. Williams, Powder bed fusion of poly(phenylene sulfide) at bed temperatures significantly below melting, *Addit. Manuf.* 28 (2019) 506–516, <https://doi.org/10.1016/j.addma.2019.05.025>.

[35] S. Berretta, K.E. Evans, O.R. Ghita, Predicting processing parameters in high temperature laser sintering (HT-LS) from powder properties, *Mater. Des.* 105 (2016) 301–314.

[36] M. Schmidt, M. Merklein, D. Bourell, D. Dimitrov, T. Hausotte, K. Wegener, L. Overmeyer, F. Vollertsen, G.N. Levy, Laser based additive manufacturing in industry and academia, *CIRP Ann.* 66 (2017) 561–583, <https://doi.org/10.1016/j.cirp.2017.05.011>.

[37] E.D. Bain, Polymer powder bed fusion additive manufacturing: recent developments in materials, processes, and applications, *Polymer-Based Additive Manufacturing: Recent Developments*, American Chemical Society, 2019, pp. 7–36, <https://doi.org/10.1021/bk-2019-1315.ch002>.

[38] T.H.C. Childs, M. Berzins, G.R. Ryder, A. Tontowi, Selective laser sintering of an amorphous polymer—simulations and experiments, *Proc. Inst. Mech. Eng. Part B* 213 (1999) 333–349, <https://doi.org/10.1243/0954405991516822>.

[39] B. Lyons, Additive manufacturing in aerospace: examples and research outlook, *National Academy of Engineering: Frontiers of Engineering: Reports on Leading-Edge Engineering from the 2011 Symposium*, The National Academies Press, Washington, DC, 2012, pp. 15–24, <https://doi.org/10.17226/13274>.

[40] B. Brule, N. Decraemer, Method for producing an object by melting a polymer powder in a powder sintering device, *US10464258B2*, 2019, <https://patents.google.com/patent/US10464258B2/en> (Accessed February 23, 2020).

[41] Y. Shi, Z. Li, H. Sun, S. Huang, F. Zeng, Effect of the properties of the polymer materials on the quality of selective laser sintering parts, *Proc. Inst. Mech. Eng. Part L* 218 (2004) 247–252.

[42] J. Frenkel, Viscous flow of crystalline bodies under the action of surface tension, *J. Phys.* 9 (1945) 385.

[43] B.N. Turner, R. Strong, S.A. Gold, A review of melt extrusion additive manufacturing processes: I. Process design and modeling, *Rapid Prototyp. J.* 20 (2014) 192–204, <https://doi.org/10.1108/RPJ-01-2013-0012>.

[44] P. Parandoush, D. Lin, A review on additive manufacturing of polymer-fiber composites, *Comp. Struct.* 182 (2017) 36–53, <https://doi.org/10.1016/j.compstruct.2017.08.088>.

[45] Titan Robotics, (n.d.). <https://titan3drobotics.com/tag/pellet-extruder/> (accessed August 22, 2019).

[46] Strangpresse Extruders, (n.d.). <http://strangpresse.com/strangpresse-extruders/> (accessed August 22, 2019).

[47] I. Gibson, D. Rosen, B. Stucker, *Additive Manufacturing Technologies: 3D Printing, Rapid Prototyping, and Direct Digital Manufacturing*, 2nd ed., Springer-Verlag, New York, 2015 (accessed April 26, 2019), <https://www.springer.com/us/book/9781493921126>.

[48] A. Bellini, S. Gucer, M. Bertoldi, Liquefier dynamics in fused deposition, *J. Manuf. Sci. Eng.* 126 (2004) 237–246.

[49] J.J. Fallon, S.H. McKnight, M.J. Bortner, Highly loaded fiber filled polymers for material extrusion: a review of current understanding, *Addit. Manuf.* (2019) 100810, , <https://doi.org/10.1016/j.addma.2019.100810>.

[50] E.L. Gilmer, D. Miller, C.A. Chatham, C. Zawaski, J.J. Fallon, A. Pekkanen, T.E. Long, C.B. Williams, M.J. Bortner, Model analysis of feedstock behavior in fused filament fabrication: enabling rapid materials screening, *Polymer* 152 (2018) 51–61, <https://doi.org/10.1016/j.polymer.2017.11.068>.

[51] M.H. Khaliq, R. Gomes, C. Fernandes, J. Nóbrega, O.S. Carneiro, L.L. Ferrás, On the use of high viscosity polymers in the fused filament fabrication process, *Rapid Prototyp. J.* 23 (2017) 727–735.

[52] Y.S. Ko, D. Herrmann, O. Tolar, W.J. Elspass, C. Brändli, Improving the filament weld-strength of fused filament fabrication products through improved inter-diffusion, *Addit. Manuf.* 29 (2019) 100815, , <https://doi.org/10.1016/j.addma.2019.100815>.

[53] S.A. Gold, B.N. Turner, A review of melt extrusion additive manufacturing processes: II. Materials, dimensional accuracy, and surface roughness, *Rapid Prototyp. J.* 21 (2015) 250–261, <https://doi.org/10.1108/RPJ-02-2013-0017>.

[54] H. Brooks, A. Rennie, T. Abram, J. McGovern, F. Caron, Variable fused deposition modelling: analysis of benefits, concept design and tool path generation, *5th International Conference on Advanced Research in Virtual and Rapid Prototyping*, Leiria, Portugal, 2011, pp. 511–517.

[55] M.E. Mackay, The importance of rheological behavior in the additive manufacturing technique material extrusion, *J. Rheol.* 62 (2018) 1549–1561, <https://doi.org/10.1122/1.5037687>.

[56] Tri-Mack, Materials | Tri-Mack Custom Plastic Parts Manufacturing. (n.d.). <http://www.trimack.com/materials> (Accessed September 11, 2019).

[57] Polyetherketone (PEK), TECAPEEK HT Black | Ensinger. (n.d.). <https://www.ensingerplastics.com/en/shapes/products/tecapeek-ht-black> (Accessed September 18, 2019).

[58] S. Hamdan, G.M. Swallowe, The strain-rate and temperature dependence of the mechanical properties of polyetherketone and polyetheretherketone, *J. Mater. Sci.* 31 (1996) 1415–1423.

[59] J. Bijwe, A.K. Kadiyala, K. Kumar, D. Puhan, T. Parida, P. Trivedi, Development of high performance poly (ether-ketone) composites based on novel processing technique, *Mater. Des.* 73 (2015) 50–59, <https://doi.org/10.1016/j.matdes.2015.02.007>.

[60] D. Defauchy, *Simulation du procédé de fabrication directe de pièces thermoplastiques par fusion laser de poudre*, PhD Thesis ENSAM, Paris, 2013.

[61] L.Q. Cortés, N. Caussé, E. Dantras, A. Lonjon, C. Lacabanne, Morphology and dynamical mechanical properties of poly ether ketone ketone (PEKK) with meta phenyl links, *J. Appl. Polym. Sci.* 133 (2016), <https://doi.org/10.1002/app.43396>.

[62] D. Gan, W. Cao, C. Song, Z. Wang, Mechanical properties and morphologies of poly (ether ketone ketone)/glass fibers/mica ternary composites, *Mater. Lett.* 51 (2001) 120–124.

[63] ASTM, Specification for Polyetherketoneketone (PEKK) Polymers for Surgical Implant Applications, ASTM International, 2015, <https://doi.org/10.1520/F2820-12>.

[64] M. Rezakazemi, M. Sadrzadeh, T. Matsuura, Thermally stable polymers for

advanced high-performance gas separation membranes, *Prog. Energy Combust. Sci.* 66 (2018) 1–41, <https://doi.org/10.1016/j.pecs.2017.11.002>.

[65] P. Wang, B. Zou, H. Xiao, S. Ding, C. Huang, Effects of printing parameters of fused deposition modeling on mechanical properties, surface quality, and microstructure of PEEK, *J. Mater. Process. Technol.* 271 (2019) 62–74, <https://doi.org/10.1016/j.jmatprotec.2019.03.016>.

[66] C.-M. Chan, S. Venkatraman, Crosslinking of poly (arylene ether ketone)s 1. Rheological behavior of the melt and mechanical properties of cured resin, *J. Appl. Polym. Sci.* 32 (1986) 5933–5943.

[67] P.J. Rae, E.N. Brown, E.B. Orler, The mechanical properties of poly (ether-ether-ketone)(PEEK) with emphasis on the large compressive strain response, *Polymer* 48 (2007) 598–615.

[68] P. Zuo, A. Tcharkhtchi, M. Shirinbayan, J. Fitoussi, F. Bakir, Overall investigation of poly (phenylene sulfide) from synthesis and process to applications—a review, *Macromol. Mater. Eng.* 304 (2019) 18000686, , <https://doi.org/10.1002/mame.201800686>.

[69] R.-C. Zhang, R. Li, A. Lu, Z. Jin, B. Liu, Z. Xu, The glass transition temperature of poly(phenylene sulfide) with various crystallinities, *Polym. Int.* 62 (2013) 449–453, <https://doi.org/10.1002/pi.4333>.

[70] J. Seppälä, M. Heino, C. Kapanen, Injection-moulded blends of a thermotropic liquid crystalline polymer with polyethylene terephthalate, polypropylene, and polyphenylene sulfide, *J. Appl. Polym. Sci.* 44 (1992) 1051–1060, <https://doi.org/10.1002/app.1992.070440614>.

[71] J.A. Brydson, *Plastics Materials*, 7th edition, Butterworth-Heinemann, Malaysia, 2013 (accessed August 24, 2019), <https://www.elsevier.com/books/plastics-materials/brydson/978-0-7506-4132-6>.

[72] H.W. Hill Jr, D.G. Brady, Properties, environmental stability, and molding characteristics of polyphenylene sulfide, *Polym. Eng. Sci.* 16 (1976) 831–835.

[73] A. Bagsik, V. Schöppner, E. Klemp, FDM part quality manufactured with Ultem® 9085, *14th International Scientific Conference on Polymeric Materials* (2010) 307–315.

[74] M.K. Pitchan, S. Bhowmik, M. Balachandran, M. Abraham, Effect of surface functionalization on mechanical properties and decomposition kinetics of high performance polyetherimide/MWCNT nano composites, *Comp. Part A* 90 (2016) 147–160, <https://doi.org/10.1016/j.compositesa.2016.06.025>.

[75] V. Francis, P.K. Jain, Advances in nanocomposite materials for additive manufacturing, *Int. J. Rapid Manuf.* 5 (2015) 215–233.

[76] H. Yang, J. Liu, M. Ji, S. Yang, Novel thermoplastic polyimide composite materials, *Thermoplastic-Composite Materials*, IntechOpen, 2012.

[77] A.R. Offringa, Thermoplastic composites—rapid processing applications, *Comp. Part A* 27 (1996) 329–336.

[78] J.H. Jia, H.D. Zhou, S.Q. Gao, J.M. Chen, A comparative investigation of the friction and wear behavior of polyimide composites under dry sliding and water-lubricated condition, *Mater. Sci. Eng. A* 356 (2003) 48–53.

[79] C. Feger, *Advances in Polyimide: Science and Technology*, CRC Press, 1993.

[80] Kira, Toray develops first ever PPS resin particles for powder bed fusion 3D printing, 3ders.Org. (n.d.). <http://www.3ders.org/articles/20160122-toray-develops-first-ever-pps-resin-powder-bed-fusion-3d-printing.html> (Accessed April 26, 2019).

[81] E. Dumoulin, *Fabrication additive de pièces en polymères thermoplastiques hautes performances et en polyamide 12 par le procédé de frittage sélectif par laser*, PhD Thesis Ecole Nationale Supérieure des Mines de Paris, 2014.

[82] M.A. Beard, O.R. Ghita, J. Bradbury, S. Flint, K.E. Evans, Material characterisation of additive manufacturing components made from a polyetherketone (PEK) high temperature thermoplastic polymer, *Innovative Developments in Virtual and Physical Prototyping*, (2011) 329–332.

[83] O.R. Ghita, E. James, R. Trimble, K.E. Evans, Physico-chemical behaviour of poly (ether ketone)(PEK) in high temperature laser sintering (HT-LS), *J. Mater. Process. Technol.* 214 (2014) 969–978.

[84] S. Berretta, Y. Wang, R. Davies, O.R. Ghita, Polymer viscosity, particle coalescence and mechanical performance in high-temperature laser sintering, *J. Mater. Sci.* 51 (2016) 4778–4794.

[85] EOS, EOS PEEK HP3, EOS GmbH - Electro Optical Systems, (2018) (Accessed April 26, 2019), <https://www.eos.info/material-p>.

[86] T. Niino, T. Uehara, Low temperature selective laser melting of high temperature plastic powder, *Proc. Solid Freeform Fabrication Symposium* (2015) 866–877.

[87] S. Berretta, K.E. Evans, O. Ghita, Processability of PEEK, a new polymer for high temperature laser sintering (HT-LS), *Eur. Polym. J.* 68 (2015) 243–266.

[88] K.H. Tan, C.K. Chua, K.F. Leong, C.M. Cheah, P. Cheang, M.S. Abu Bakar, S.W. Cha, Scaffold development using selective laser sintering of polyetheretherketone-hydroxyapatite biocomposite blends, *Biomaterials* 24 (2003) 3115–3123, [https://doi.org/10.1016/S0142-9612\(03\)00131-5](https://doi.org/10.1016/S0142-9612(03)00131-5).

[89] T.J. Hoskins, K.D. Dearn, S.N. Kukureka, Mechanical performance of PEEK produced by additive manufacturing, *Polym. Test.* 70 (2018) 511–519, <https://doi.org/10.1016/j.polymertesting.2018.08.008>.

[90] M. Yan, X. Tian, G. Peng, D. Li, X. Zhang, High temperature rheological behavior and sintering kinetics of CF/PEEK composites during selective laser sintering, *Comp. Sci. Technol.* 165 (2018) 140–147.

[91] M. Kroh, C. Bonten, P. Eyerer, Influences on morphology in laser sintered PEEK materials, *Proceedings of the Polymer Processing Society 28th Annual Meeting*, Pattaya, Thailand, 2012.

[92] F. Ito, T. Niino, Implementation of Top Hat profile laser into Low temperature process of poly phenylene sulfide, *Proc. 27th Annual International Solid Freeform Fabrication Symposium* (2016) 2194–2203.

[93] G. Vaganov, A. Didenko, E. Ivan'kova, E. Popova, V. Yudin, V. Elokhovskii, I. Lasota, Development of new polyimide powder for selective laser sintering, *J. Mater. Res.* 34 (2019) 2895–2902, <https://doi.org/10.1557/jmr.2019.161>.

[94] M. Dawoud, I. Taha, S.J. Ebeid, Mechanical behaviour of ABS: an experimental study using FDM and injection moulding techniques, *J. Manuf. Processes.* 21 (2016) 39–45.

[95] A.R. Torrado, C.M. Shemelya, J.D. English, Y. Lin, R.B. Wicker, D.A. Roberson, Characterizing the effect of additives to ABS on the mechanical property anisotropy of specimens fabricated by material extrusion 3D printing, *Addit. Manuf.* 6 (2015) 16–29.

[96] B. Wittbrodt, J.M. Pearce, The effects of PLA color on material properties of 3-D printed components, *Addit. Manuf.* 8 (2015) 110–116.

[97] L. Suryanegara, A.N. Nakagaito, H. Yano, The effect of crystallization of PLA on the thermal and mechanical properties of microfibrillated cellulose-reinforced PLA composites, *Comp. Sci. Technol.* 69 (2009) 1187–1192.

[98] S.-K. Yeh, S. Agarwal, R.K. Gupta, Wood-plastic composites formulated with virgin and recycled ABS, *Comp. Sci. Technol.* 69 (2009) 2225–2230.

[99] M. Rubenstein, R.H. Colby, *Polymer Physics*, Oxford University Press, New York, 2003.

[100] P.C. Painter, M.M. Coleman, *Essentials of Polymer Science and Engineering*, DEStech Publications, Inc, 2008.

[101] A. Das, A.E.C. Marnot, J.J. Fallon, S.M. Martin, E.G. Joseph, M.J. Bortner, Material extrusion-based additive manufacturing with blends of polypropylene and hydrocarbon resins, *ACS Appl. Polym. Mater.* 2 (2020) 911–921, <https://doi.org/10.1021/acsm.apm.9b01127>.

[102] B. Brenken, E. Barocio, A. Favoloro, V. Kunc, R.B. Pipes, Development and validation of extrusion deposition additive manufacturing process simulations, *Addit. Manuf.* 25 (2019) 218–226.

[103] Y.M. Boiko, G. Guérin, V.A. Marikhin, R.E. Prud'homme, Healing of interfaces of amorphous and semi-crystalline poly (ethylene terephthalate) in the vicinity of the glass transition temperature, *Polymer* 42 (2001) 8695–8702.

[104] B.-R. Cho, J.L. Kardos, Consolidation and self-bonding in poly (ether ether ketone) (PEEK), *J. Appl. Polym. Sci.* 56 (1995) 1435–1454.

[105] F. Awaja, S. Zhang, Self-bonding of PEEK for active medical implants applications, *J. Adhes. Sci. Technol.* 29 (2015) 1593–1606.

[106] C. Bonten, E. Schmachtenberg, A new hypothesis to describe the mechanisms acting in a welded joint of semicrystalline thermoplastics, *Polym. Eng. Sci.* 41 (2001) 475–483.

[107] Y.-Q. Xue, T.A. Tervoort, S. Rastogi, J. Lemstra, Welding behavior of semicrystalline polymers. 2. Effect of cocrystallization on autoadhesion, *Macromolecules* 33 (2000) 7084–7087.

[108] T. Schuman, E.V. Stepanov, S. Nazarenko, G. Capaccio, A. Hiltner, E. Baer, Interdiffusion of linear and branched polyethylene in microlayers studied via melting behavior, *Macromolecules* 31 (1998) 4551–4561.

[109] C. Yang, X. Tian, D. Li, Y. Cao, F. Zhao, C. Shi, Influence of thermal processing conditions in 3D printing on the crystallinity and mechanical properties of PEEK material, *J. Mater. Process. Technol.* 248 (2017) 1–7.

[110] M. Rinaldi, T. Ghidini, F. Cecchini, A. Brandao, F. Nanni, Additive layer manufacturing of poly (ether ether ketone) via FDM, *Comp. Part B* 145 (2018) 162–172.

[111] W. Wu, P. Geng, G. Li, D. Zhao, H. Zhang, J. Zhao, Influence of layer thickness and raster angle on the mechanical properties of 3D-printed PEEK and a comparative mechanical study between PEEK and ABS, *Materials* 8 (2015) 5834–5846.

[112] G. Cicala, A. Latteri, B. Del Curto, A. Lo Russo, G. Recca, S. Farè, Engineering thermoplastics for additive manufacturing: a critical perspective with experimental evidence to support functional applications, *J. Appl. Biomater. Funct. Mater.* 15 (2017) 10–18.

[113] K.M. Rahman, T. Letcher, R. Reese, Mechanical properties of additively manufactured peek components using fused filament fabrication, *ASME 2015 International Mechanical Engineering Congress and Exposition*, American Society of Mechanical Engineers, Houston, Texas, 2015 p. V02AT02A009.

[114] R. Wang, K. Cheng, R.C. Advincula, Q. Chen, On the thermal processing and mechanical properties of 3D-printed polyether ether ketone, *MRS Commun.* (un-defined/ed) 1–7. <https://doi.org/10.1557/mrc.2019.86>.

[115] X. Deng, Z. Zeng, B. Peng, S. Yan, W. Ke, Mechanical properties optimization of poly-ether-ether-ketone via fused deposition modeling, *Materials* 11 (2018) 216.

[116] M. Vaezi, S. Yang, Extrusion-based additive manufacturing of PEEK for biomedical applications, *Virt. Phys. Prototyp.* 10 (2015) 123–135, <https://doi.org/10.1080/17452759.2015.1097053>.

[117] M.F. Arif, S. Kumar, K.M. Varadarajan, W.J. Cantwell, Performance of biocompatible PEEK processed by fused deposition additive manufacturing, *Mater. Des.* 146 (2018) 249–259.

[118] R. Davies, Y. Wang, O. Ghita, Extrusion deposition of carbon nanotubes (CNT)/poly ether ether ketone (PEEK), *20th International Conference on Composite Materials* (2015).

[119] S. Berretta, R. Davies, Y.T. Shyng, Y. Wang, O. Ghita, Fused deposition modelling of high temperature polymers: exploring CNT PEEK composites, *Polym. Test.* 63 (2017) 251–262.

[120] X. Han, D. Yang, C. Yang, S. Spintzyk, L. Scheideler, P. Li, D. Li, J. Geis-Gerstorfer, F. Rupp, Carbon fiber reinforced PEEK composites based on 3D-printing technology for orthopedic and dental Applications, *J. Clin. Med.* 8 (2019) 240.

[121] R. Velu, N. Vaheed, M.K. Ramachandran, F. Raspall, Experimental investigation of robotic 3D printing of high-performance thermoplastics (PEEK): a critical perspective to support automated fibre placement process, *Int. J. Adv. Manuf. Technol.* (2019), <https://doi.org/10.1007/s00170-019-04623-z>.

[122] M.F. Arif, H. Alhashmi, K.M. Varadarajan, J.H. Koo, A.J. Hart, S. Kumar, Multifunctional performance of carbon nanotubes and graphene nanoplatelets reinforced PEEK composites enabled via FFF additive manufacturing, *Comp. Part B* (2019) 107625, , <https://doi.org/10.1016/j.compositesb.2019.107625>.

[123] A.E. Magri, K.E. Mabrouk, S. Vaudreuil, H. Chibane, M.E. Touhami, Optimization of printing parameters for improvement of mechanical and thermal performances of 3D printed poly(ether ether ketone) parts, *J. Appl. Polym. Sci.* (2020) e49087, , <https://doi.org/10.1002/app.49087>.

[124] K.C. Chuang, J.E. Grady, R.D. Draper, E.-S.E. Shin, C. Patterson, T.D. Santelle, Additive manufacturing and characterization of ultem polymers and composites, CAMX Conference Proceedings, Dallas, TX, 2015.

[125] I.V. Polyakov, G.V. Vaganov, V.E. Yudin, E.M. Ivan'kova, E.N. Popova, V.Y. Elokhovskii, Investigation of properties of nanocomposite polyimide samples obtained by fused deposition modeling, *Mech. Comp. Mater.* 54 (2018) 33–40.

[126] M. Fischer, V. Schöppner, Fatigue behavior of FDM parts manufactured with Ultem 9085, *JOM* 69 (2017) 563–568.

[127] R.J. Zaldivar, D.B. Witkin, T. McLouth, D.N. Patel, K. Schmitt, J.P. Nokes, Influence of processing and orientation print effects on the mechanical and thermal behavior of 3D-printed ULTEM® 9085 material, *Addit. Manuf.* 13 (2017) 71–80.

[128] K.I. Byberg, A.W. Gebisa, H.G. Lemu, Mechanical properties of ULTEM 9085 material processed by fused deposition modeling, *Polym. Test.* 72 (2018) 335–347, <https://doi.org/10.1016/j.polymertesting.2018.10.040>.

[129] J.M. Gardner, G. Sauti, J.-W. Kim, R.J. Cano, R.A. Wincheski, C.J. Stelter, B.W. Grimsley, D.C. Working, E.J. Siochi, 3-D printing of multifunctional carbon nanotube yarn reinforced components, *Addit. Manuf.* 12 (2016) 38–44.

[130] C.E. Duty, V. Kunc, B. Compton, B. Post, D. Erdman, R. Smith, R. Lind, P. Lloyd, L. Love, Structure and mechanical behavior of Big Area Additive Manufacturing (BAAM) materials, *Rapid Prototyp. J.* 23 (2017) 181–189.

[131] E.R. Fitzharris, I. Watt, D.W. Rosen, M.L. Shofner, Interlayer bonding improvement of material extrusion parts with polyphenylene sulfide using the Taguchi method, *Addit. Manuf.* 24 (2018) 287–297.

[132] A.A. Hassen, J. Lindahl, X. Chen, B. Post, L. Love, V. Kunc, Additive manufacturing of composite tooling using high temperature thermoplastic materials, SAMPE Conference Proceedings, Long Beach, CA, 2016, pp. 23–26.

[133] P. Geng, J. Zhao, W. Wu, Y. Wang, B. Wang, S. Wang, G. Li, Effect of thermal processing and heat treatment condition on 3D printing PPS properties, *Polymers* 10 (2018) 875.

[134] N.M. DeNardo, Additive Manufacturing of Carbon Fiber-Reinforced Thermoplastic Composites, Master of Science Thesis Purdue University, 2016.

[135] M.Q. Ansari, M.J. Bortner, D.G. Baird, Generation of polyphenylene sulfide reinforced with a thermotropic liquid crystalline polymer for application in fused filament fabrication, *Addit. Manuf.* 29 (2019) 100814, , <https://doi.org/10.1016/j.addma.2019.100814>.

[136] J.N. Hay, D.J. Kemmish, Thermal decomposition of poly (aryl ether ketones), *Polymer* 28 (1987) 2047–2051.

[137] B. Chen, S. Berretta, R. Davies, O. Ghita, Characterisation of carbon fibre (Cf) - Poly Ether Ketone (PEK) composite powders for laser sintering, *Polym. Test.* 76 (2019) 65–72, <https://doi.org/10.1016/j.polymertesting.2019.03.011>.

[138] V. Kishore, X. Chen, C. Ajinjeru, A.A. Hassen, J.M. Lindahl, J. Failla, V. Kunc, C.E. Duty, Additive manufacturing of high performance semicrystalline thermoplastics and their composites, Proc. 27th Annual International Solid Freeform Fabrication Symposium, Austin, TX, 2016, pp. 906–915.

[139] V. Kishore, C. Ajinjeru, C.E. Duty, A.A. Hassen, J.M. Lindahl, P. Liu, V. Kunc, Rheological characteristics of fiber reinforced poly (ether ketone ketone)(PEKK) for melt extrusion additive manufacturing, SAMPE Conference Proceedings, Seattle, WA, 2017.

[140] C. Ajinjeru, V. Kishore, P. Liu, A.A. Hassen, J.M. Lindahl, V. Kunc, C.E. Duty, Rheological Evaluation of High Temperature Polymers to Identify Successful Extrusion Parameters, Oak Ridge National Lab.(ORNL), Oak Ridge, TN (United States), 2017.

[141] V. Kishore, C. Ajinjeru, P. Liu, J. Lindahl, A. Hassen, V. Kunc, C. Duty, Predicting sharkskin instability in extrusion additive manufacturing of reinforced thermoplastics, Proceedings of Solid Freeform Fabrication Symposium, Austin, TX, 2017, pp. 1696–1704.

[142] V. Kunc, V. Kishore, X. Chen, C. Ajinjeru, C. Duty, A.A. Hassen, High Performance Poly(Etherketoneketone) (PEKK) Composite Parts Fabricated Using Big Area Additive Manufacturing (BAAM) Processes, Oak Ridge National Lab. (ORNL), Oak Ridge, TN (United States). Manufacturing Demonstration Facility (MDF), 2016, <https://doi.org/10.2172/1343535>.

[143] B. Jackson, EOS Releases Aerospace Grade PEKK 3D Printer Material in Collaboration With Boeing, 3D Printing Industry, (2018) (accessed February 24, 2020), <https://3dprintingindustry.com/news/eos-releases-aerospace-grade-pekk-3d-printer-material-collaboration-boeing-132469/>.

[144] A. Lo, Hexcel Makes Boeing's Qualified Provider List for 3D Printed Aircraft Components, 3D Printing Industry, (2019) (Accessed February 24, 2020), <https://3dprintingindustry.com/news/hexcel-makes-boeings-qualified-provider-list-for-3d-printed-aircraft-components-160887/>.

[145] M. Molitch-Hou, OPM Brings Two PEKK 3D Printing Materials to Aerospace Market, Oxford Performance Materials, (2014) (Accessed February 24, 2020), <http://oxfordpm.com/news-events/opp-in-the-news?id=339648/opp-brings-two-pekk-3d-printing-materials-to-aerospace-market>.

[146] America Makes 4006, Maturation of High-Temperature SLS Technologies & Infrastructure. (n.d.). <https://www.americamakes.us/portfolio/4006-maturation-high-temperature-selective-laser-sintering-sls-technologies-infrastructure/> (Accessed February 23, 2020).

[147] P. Peyre, Y. Rouchausse, D. Defauchy, G. Régnier, Experimental and numerical analysis of the selective laser sintering (SLS) of PA12 and PEKK semi-crystalline polymers, *J. Mater. Process. Technol.* 225 (2015) 326–336.

[148] L. Benedetti, B. Brûlé, N. Decreamer, K.E. Evans, O. Ghita, Shrinkage behaviour of semi-crystalline polymers in laser sintering: PEKK and PA12, *Mater. Des.* 181 (2019) 107906, , <https://doi.org/10.1016/j.matdes.2019.107906>.

[149] T. Choupin, B. Fayolle, G. Régnier, C. Paris, J. Cinquin, B. Brûlé, Isothermal crystallization kinetic modeling of poly(etherketoneketone) (PEKK) copolymer, *Polymer* 111 (2017) 73–82, <https://doi.org/10.1016/j.polymer.2017.01.033>.

[150] S. Fischer, A. Pfister, V. Galitz, B. Lyons, C.V. Robinson, K. Rupel, R. Booth, S. Kubiak, A high-performance material for aerospace applications : development of carbon fiber filled PEKK for laser sintering, *Proceedings of the 26th Annual International Solid Freeform Fabrication Symposium*, Austin, TX, 2016, pp. 808–813.

[151] C. Mielicki, A. Wegner, B. Gronhoff, J. Wortberg, G. Witt, Prediction of PA12 melt viscosity in laser sintering by a time and temperature dependent rheological model, *RTEjournal* 32 (2012).

[152] Northrop Grumman Aerospace Systems, Oxford Performance Materials, Applied Science & Technology Transfer, 3D Systems & Arkema, America Makes, Statistically Significant PEKK Properties Developed, (2015) (Accessed February 24, 2020), https://www.americamakes.us/wp-content/uploads/sites/2/2017/07/4006_SuccessStory.pdf.

[153] K.H. Tan, C.K. Chua, K.F. Leong, M.W. Naing, C.M. Cheah, Fabrication and characterization of three-dimensional poly (ether-ether-ketone)-hydroxyapatite biocomposite scaffolds using laser sintering, *Proc. Inst. Mech. Eng.* 219 (2005) 183–194.

[154] A. Mazzoli, Selective laser sintering in biomedical engineering, *Med. Biol. Eng. Comput.* 51 (2013) 245–256.

[155] M. Schmidt, D. Pohle, T. Rechtenwald, Selective laser sintering of PEEK, *CIRP Ann.* 56 (2007) 205–208.

[156] T. Rechtenwald, G. E\sser, M. Schmidt, D. Pohle, Comparison between Laser Sintering of PEEK and PA using design of experiment methods, *Virtual Modelling and Rapid Manufacturing: Advanced Research in Virtual and Rapid Prototyping*, CRC Press, Leiria, Portugal, 2005, pp. 343–348.

[157] B. Chen, S. Berretta, K. Evans, K. Smith, O. Ghita, A primary study into graphene/polyether ether ketone (PEEK) nanocomposite for laser sintering, *Appl. Surf. Sci.* 428 (2018) 1018–1028.

[158] B. Valentan, Z. Kadivnik, T. Brajlih, A. Anderson, I. Drstvensek, Processing poly (ether etherketone) on a 3D printer for thermoplastic modelling, *Mater. Technol.* 47 (2013) 715–721.

[159] A. Haleem, M. Javaid, Polyether ether ketone (PEEK) and its manufacturing of customised 3D printed dentistry parts using additive manufacturing, *Clin. Epidemiol. Global Health* 7 (2019) 654–660, <https://doi.org/10.1016/j.cegh.2019.03.001>.

[160] W.Z. Wu, P. Geng, J. Zhao, Y. Zhang, D.W. Rosen, H.B. Zhang, Manufacture and thermal deformation analysis of semicrystalline polymer polyether ether ketone by 3D printing, *Mater. Res. Innov.* 18 (2014) S5–12.

[161] C.-Y. Liao, P.-L. Wu, C.-Y. Lee, Customized PEEK implants with microporous and surface modification using 3D printing, *American Society of Mechanical Engineers Digital Collection*, (2019), <https://doi.org/10.1115/DETC2019-97117>.

[162] S. Ding, B. Zou, P. Wang, H. Ding, Effects of nozzle temperature and building orientation on mechanical properties and microstructure of PEEK and PEI printed by 3D-FDM, *Polym. Test.* 78 (2019) 105948, , <https://doi.org/10.1016/j.polymertesting.2019.105948>.

[163] C. Basgul, T. Yu, D.W. MacDonald, R. Siske, M. Marcolongo, S.M. Kurtz, Does annealing improve the interlayer adhesion and structural integrity of FFF 3D printed PEEK lumbar spinal cages? *J. Mech. Behav. Biomed. Mater.* 102 (2020) 103455, , <https://doi.org/10.1016/j.jmbbm.2019.103455>.

[164] M. Chapiro, Current achievements and future outlook for composites in 3D printing, *Reinforced Plast.* 60 (2016) 372–375, <https://doi.org/10.1016/j.repl.2016.10.002>.

[165] E.R. Fitzharris, N. Watanabe, D.W. Rosen, M.L. Shofner, Effects of material properties on warpage in fused deposition modeling parts, *Int. J. Adv. Manuf. Technol.* 95 (2018) 2059–2070.

[166] A.C. de Leon, Q. Chen, N.B. Palaganas, J.O. Palaganas, J. Manapat, R.C. Advincula, High performance polymer nanocomposites for additive manufacturing applications, *React. Funct. Polym.* 103 (2016) 141–155.

[167] StarShape, (n.d.). <https://www.coherent.com/lasers/laser/starshape-300-450-650-performance> (Accessed September 11, 2019).

[168] V.E. Yudin, V.M. Svetlichny, Carbon plastics based on thermoplastic polyimide binders modified with nanoparticles, *Polym. Sci. Ser. C* 58 (2016) 16–25, <https://doi.org/10.1134/S1811238216010124>.

[169] A.C. de Bruijn, G. Gómez-Gras, M.A. Pérez, Mechanical study on the impact of an effective solvent support-removal methodology for FDM Ultem 9085 parts, *Polym. Test.* (2020) 106433, <https://doi.org/10.1016/j.polymertesting.2020.106433>.

[170] H. Wu, M. Sulkis, J. Driver, A. Saade-Castillo, A. Thompson, J.H. Koo, Multi-functional ULTEM® 1010 composite filaments for additive manufacturing using fused filament fabrication (FFF), *Addit. Manuf.* 24 (2018) 298–306.

[171] G. Taylor, X. Wang, L. Mason, M.C. Leu, K. Chandrashekhar, T. Schniepp, R. Jones, Flexural behavior of additively manufactured Ultem 1010: experiment and simulation, *Rapid Prototyp. J.* 24 (2018) 1003–1011, <https://doi.org/10.1108/RPJ-02-2018-0037>.

[172] G. Taylor, S. Anandan, D. Murphy, M. Leu, K. Chandrashekhar, T. Schniepp, R. Jones, Flexural behavior of additively manufactured ULTEM 1010, *Virt. Phys. Prototyp.* 14 (2019) 277–283, <https://doi.org/10.1080/17452759.2018.1558494>.

[173] P. Han, A. Tofangchi, A. Deshpande, S. Zhang, K. Hsu, An approach to improve interface healing in FFF-3D printed Ultem 1010 using laser pre-deposition heating, *Procedia Manuf.* 34 (2019) 672–677, <https://doi.org/10.1016/j.promfg.2019.06.195>.

[174] O. Kaynan, A. Yildiz, Y.E. Bozkurt, E.O. Yenigun, H. Cebeci, Development of Multifunctional CNTs Reinforced PEI Filaments for Fused Deposition Modeling, in:

AIAA Scitech 2019 Forum, American Institute of Aeronautics and Astronautics, n.d. <https://doi.org/10.2514/6.2019-0406>.

[175] W. Wu, W. Ye, P. Geng, Y. Wang, G. Li, X. Hu, J. Zhao, 3D printing of thermoplastic PI and interlayer bonding evaluation, *Mater. Lett.* 229 (2018) 206–209.

[176] C. Ajinjeru, V. Kishore, X. Chen, J. Lindahl, Z. Sudbury, A.A. Hassen, V. Kunc, B. Post, L. Love, C. Duty, The influence of rheology on melt processing conditions of amorphous thermoplastics for big area additive manufacturing (BAAM), 27th Annual International Solid Freeform Fabrication Symposium, Austin, TX, 2016, pp. 754–762.

[177] I. Blanco, G. Cicala, G. Ognibene, M. Rapisarda, A. Recca, Thermal properties of polyetherimide/polycarbonate blends for advanced applications, *Polym. Degrad. Stab.* 154 (2018) 234–238, <https://doi.org/10.1016/j.polymdegradstab.2018.06.011>.

[178] America Makes 3003, High Performance Additive Manufactured Thermoplastics. (n.d.). <https://www.americamakes.us/portfolio/3003-high-performance-additive-manufactured-thermoplastics/> (Accessed September 11, 2019).

[179] A. Almabrouk Mousa, Experimental investigations of curling phenomenon in selective laser sintering process, *Rapid Prototyp. J.* 22 (2016) 405–415.

[180] M. Drexler, M. Lexow, D. Drummer, Selective laser melting of polymer Powder-Part mechanics as function of exposure speed, *Phys. Procedia* 78 (2015) 328–336.

[181] S. Fish, J.C. Booth, S.T. Kubiak, W.W. Wroe, A.D. Bryant, D.R. Moser, J.J. Beaman, Design and subsystem development of a high temperature selective laser sintering machine for enhanced process monitoring and control, *Addit. Manuf.* 5 (2015) 60–67.

[182] W.J. Swanson, P.W. Turley, P.J. Leavitt, P.J. Karwoski, J.E. LaBossiere, R.L. Skubic, High temperature modeling apparatus, 6,722,872, 2004.

[183] W.J. Swanson, P.W. Turley, P.J. Leavitt, P.J. Karwoski, J.E. LaBossiere, R.L. Skubic, High-temperature modeling method, 7,297,304, 2007.

[184] J.-W. Tseng, C.-Y. Liu, Y.-K. Yen, J. Bellkner, T. Bremicker, B.H. Liu, T.-J. Sun, A.-B. Wang, Screw extrusion-based additive manufacturing of PEEK, *Mater. Des.* 140 (2018) 209–221, <https://doi.org/10.1016/j.matdes.2017.11.032>.

[185] A.A. Stepankin, D.I. Chukov, F.S. Senatov, A.I. Salimon, A.M. Korsunsky, S.D. Kaloshkin, 3D-printed PEEK-carbon fiber (CF) composites: structure and thermal properties, *Comp. Sci. Technol.* 164 (2018) 319–326.

[186] P. Geng, J. Zhao, W. Wu, W. Ye, Y. Wang, S. Wang, S. Zhang, Effects of extrusion speed and printing speed on the 3D printing stability of extruded PEEK filament, *J. Manuf. Processes* 37 (2019) 266–273, <https://doi.org/10.1016/j.jmapro.2018.11.023>.

[187] C. Zawaski, C. Williams, Design of a low-cost, high-temperature inverted build environment to enable desktop-scale additive manufacturing of performance polymers, *Addit. Manuf.* (2020) 101111, <https://doi.org/10.1016/j.addma.2020.101111>.

[188] J.M. Gardner, C.J. Stelter, E.A. Yashin, E.J. Siochi, High Temperature Thermoplastic Additive Manufacturing Using Low-Cost, Open-Source Hardware, (2016).

[189] E.L. Gilmer, C. Mansfield, J.M. Gardner, E.J. Siochi, D.G. Baird, M.J. Bortner, Characterization and analysis of polyetherimide: realizing practical challenges of modeling the extrusion-based additive manufacturing process, *Polymer-Based Additive Manufacturing: Recent Developments*, ACS Books, 2019.

[190] C.-U. Lee, A.J. Boydston, M.A. Ganter, D.W. Storti, Additive Manufacturing Using Photothermal Dyes for High Efficiency Sintering, US20190275735A1, 2019.

<https://patents.google.com/patent/US20190275735A1/en> (Accessed February 24, 2020).

[191] S. Berretta, O. Ghita, K.E. Evans, Morphology of polymeric powders in Laser Sintering (LS): from polyamide to new PEEK powders, *Eur. Polym. J.* 59 (2014) 218–229.

[192] D.A. Anderegg, H.A. Bryant, D.C. Ruffin, S.M. Skrip Jr, J.J. Fallon, E.L. Gilmer, M.J. Bortner, In-situ monitoring of polymer flow temperature and pressure in extrusion based additive manufacturing, *Addit. Manuf.* 26 (2019) 76–83.

[193] T.J. Coogan, D.O. Kazmer, In-line rheological monitoring of fused deposition modeling, *J. Rheol.* 63 (2019) 141–155.

[194] J.E. Seppala, K.D. Migler, Infrared thermography of welding zones produced by polymer extrusion additive manufacturing, *Addit. Manuf.* 12 (2016) 71–76.

[195] R.B. Dinwiddie, V. Kunc, J.M. Lindal, B. Post, R.J. Smith, L. Love, C.E. Duty, Infrared imaging of the polymer 3D-printing process, Thermosense: Thermal Infrared Applications XXXVI, International Society for Optics and Photonics, Baltimore, Maryland, United States, 2014, <https://doi.org/10.1117/12.2053425> 910502.

[196] Best PEEK 3D printer PEI Ultem, Aniwaa. (n.d.). <https://www.aniwaa.com/best-peek-3d-printer-pei-ultem/> (Accessed October 8, 2019).

[197] N. Watanabe, M. Shofner, N. Treat, D. Rosen, A model for residual stress and part warpage prediction in material extrusion with application to polypropylene, 2016 Annual International Solid Freeform Fabrication Symposium, Austin (2016).

[198] Y. Yan, R. Zhang, G. Hong, X. Yuan, Research on the bonding of material paths in melted extrusion modeling, *Mater. Des.* 21 (2000) 93–99.

[199] S. Sinha, N.A. Meisel, Influence of embedding process on mechanical properties of material extrusion parts, *Proceedings of the 27th Annual International Solid Freeform Fabrication Symposium Freeform Fabrication* (2016) 847–863.

[200] M. Spoerk, J. Sapkota, G. Weingrill, T. Fischinger, F. Arbeiter, C. Holzer, Shrinkage and warpage optimization of expanded-perlite-filled polypropylene composites in extrusion-based additive manufacturing, *Macromol. Mater. Eng.* 302 (2017) 1700143.

[201] S.F. Costa, F.M. Duarte, J.A. Covas, Thermal conditions affecting heat transfer in FDM/FFE: a contribution towards the numerical modelling of the process: this paper investigates convection, conduction and radiation phenomena in the filament deposition process, *Virt. Phys. Prototyp.* 10 (2015) 35–46.

[202] C. Ajinjeru, V. Kishore, J. Lindahl, Z. Sudbury, A.A. Hassen, B. Post, L. Love, V. Kunc, C. Duty, The influence of dynamic rheological properties on carbon fiber-reinforced polyetherimide for large-scale extrusion-based additive manufacturing, *Int. J. Adv. Manuf. Technol.* 99 (2018) 411–418, <https://doi.org/10.1007/s00170-018-2510-z>.

[203] K. Prashantha, F. Roger, Multifunctional properties of 3D printed poly (lactic acid)/graphene nanocomposites by fused deposition modeling, *J. Macromol. Sci. Part A* 54 (2017) 24–29.

[204] S. Dul, L. Fambri, A. Pegoretti, Fused deposition modelling with ABS-graphene nanocomposites, *Comp. Part A* 85 (2016) 181–191.

[205] W.W. Yu, J. Zhang, J.R. Wu, X.Z. Wang, Y.H. Deng, Incorporation of graphitic nano-filler and poly (lactic acid) in fused deposition modeling, *J. Appl. Polym. Sci.* 134 (2017).

[206] L.J. Love, V. Kunc, O. Rios, C.E. Duty, A.M. Elliott, B.K. Post, R.J. Smith, C.A. Blue, The importance of carbon fiber to polymer additive manufacturing, *J. Mater. Res.* 29 (2014) 1893–1898.